Reynolds stress closure for nonequilibrium effects in turbulent flows

Peter E. Hamlington[a] and Werner J. A. Dahm
Laboratory for Turbulence and Combustion (LTC), Department of Aerospace Engineering, The University of Michigan, Ann Arbor, Michigan 48109-2140, USA

(Received 7 March 2008; accepted 15 September 2008; published online 5 November 2008)

From consideration of turbulence anisotropy dynamics due to spatial or temporal variations in the mean strain rate, a new Reynolds stress closure for nonequilibrium effects in turbulent flows has been developed. This closure, formally derived from the Reynolds stress anisotropy transport equation, results in an effective strain rate tensor that accounts for the strain rate history to which the turbulence has been subjected. In contrast to prior nonequilibrium models that have sought to address nonequilibrium effects via changes in the eddy viscosity, the present approach accounts for nonequilibrium effects in the fundamental relation between the anisotropy tensor and the strain rate tensor. The time-local form of the nonequilibrium closure can be readily implemented in place of the classical equilibrium Boussinesq closure on which most existing computational frameworks are currently based. This new closure is applied here to four substantially different classes of nonequilibrium test problems. Results show dramatically improved agreement with experimental and computational data, without the need to vary any model parameters, when compared with the standard equilibrium closure and with various prior nonequilibrium closures. © *2008 American Institute of Physics*. [DOI: 10.1063/1.3006023]

I. INTRODUCTION

Due to the overwhelming computational resources needed for direct numerical simulations (DNSs) of essentially all practical engineering turbulent flow problems—and even for true large eddy simulations (LESs) of most such problems—the vast majority of simulations for these types of flows will continue for the foreseeable future to be done within the steady or unsteady Reynolds-averaged Navier–Stokes (RANS) framework. We will deal here for purposes of clarity with incompressible turbulent flows. Averaging the continuity and momentum equations leads to the first-order single-point moment equations for the mean-flow velocity components $\bar{u}_i(\mathbf{x},t)$ and kinematic pressure $\bar{p}(\mathbf{x},t)$, namely,

$$\frac{\partial \bar{u}_i}{\partial x_i} = 0, \tag{1}$$

$$\frac{D\bar{u}_i}{Dt} = -\frac{\partial \bar{p}}{\partial x_i} + \frac{\partial}{\partial x_j}[2\nu \bar{S}_{ij} - \overline{u_i' u_j'}], \tag{2}$$

where $D/Dt \equiv \partial/\partial t + \bar{u}_j \partial/\partial x_j$ denotes the mean-flow material derivative, and

$$\bar{S}_{ij} \equiv \frac{1}{2}\left(\frac{\partial \bar{u}_i}{\partial x_j} + \frac{\partial \bar{u}_j}{\partial x_i}\right) \tag{3}$$

is the mean strain rate tensor. The overbar in Eqs. (1)–(3) and elsewhere herein is understood to be an ensemble average at location $\mathbf{x}$ and time t over infinitely many realizations of the "same" turbulent flow having nominally identical initial and boundary conditions, despite the fact that this average is often implemented in practice via time or space averaging. The ensemble average interpretation will become important for the nonequilibrium anisotropy closure developed herein.

Solving Eqs. (1)–(3) requires a closure representation for the Reynolds stresses $\overline{u_i' u_j'}$ in Eq. (2), where primes denote fluctuations relative to the average. This stress tensor can be written in terms of its isotropic form $\frac{2}{3}k\delta_{ij}$ and the deviations from isotropy as

$$\overline{u_i' u_j'} = \tfrac{2}{3}k\delta_{ij} - (\overline{u_i' u_j'})_{\text{dev}}, \tag{4}$$

where $k \equiv \frac{1}{2}\overline{u_i' u_i'}$ is the turbulence kinetic energy. The anisotropic part $(\overline{u_i' u_j'})_{\text{dev}}$ can be equivalently expressed in terms of the Reynolds stress anisotropy tensor

$$a_{ij} \equiv -\frac{(\overline{u_i' u_j'})_{\text{dev}}}{k}. \tag{5}$$

The closure required in Eqs. (1)–(4) thus amounts to constructing a representation for the anisotropy tensor a_{ij} in Eq. (5). It has been a major goal of fluid dynamics research for well over a century to develop such a closure model that is reliably accurate over the range of conditions encountered in essentially all practical problems.

A. Classical equilibrium anisotropy closure

The most widely used turbulence models are formulated in a framework that introduces the required closure directly at the level of the second-order single-point moments $\overline{u_i' u_j'}$. Nearly all of these are based on the classical equilibrium Boussinesq hypothesis, first introduced in 1877, that assumes the deviatoric stresses in Eq. (4) to be directly proportional to the mean strain rate $\bar{S}_{ij}$ in Eq. (3), namely, $(\overline{u_i' u_j'})_{\text{dev}} \sim \bar{S}_{ij}$. The corresponding anisotropy tensor in Eq. (5) is then

[a]Author to whom correspondence should be addressed. Electronic mail: peterha@umich.edu.

$$a_{ij} = -2\frac{\nu_T}{k}\bar{S}_{ij}, \tag{6}$$

where ν_T is an eddy viscosity that must itself be modeled, often with a two-equation formulation, to complete the closure. The vast majority of such two-equation turbulence models differ primarily in how they choose to represent ν_T but fundamentally are based on the equilibrium assumption in Eq. (6) that the anisotropy is proportional to the *local instantaneous* mean strain rate tensor $\bar{S}_{ij}$.

The inaccuracies of all such "direct Reynolds stress models" that have been proposed to date are well known.[1–3] As a consequence, for at least the past decade or more, most research has focused elsewhere in seeking improved turbulence models. Today, the most accurate closure approaches do not represent the Reynolds stresses directly as in Eq. (6) but instead couple Eqs. (1)–(3) with the system of second-order single-point moment equations for the six independent components of $\overline{u_i' u_j'}$, or equivalently a_{ij}, in what are termed "Reynolds stress transport models." In principle, the additional partial differential equations involved in such approaches contain all of the relevant dynamics that affect the Reynolds stress anisotropy tensor a_{ij}. In practice, however, these transport equations involve many terms that must be modeled, some with Boussinesq-like equilibrium representations that are analogous to Eq. (6). Moreover, numerical integration of the six additional coupled partial differential equations increases the computational requirements and introduces stability issues associated with solving Eqs. (1)–(3), often to such an extent that this approach can be prohibitive for many practical situations.

Due to their substantially greater computational simplicity, direct approaches for representing the anisotropy a_{ij} based on modifications to the equilibrium closure in Eq. (6), often by changing how the eddy viscosity ν_T is modeled, have found more widespread use. Sometimes, the linear Boussinesq representation is replaced with a general tensorial expansion in powers of the mean strain rate and rotation rate tensors. Such nonlinear eddy viscosity approaches[4–7] retain most of the computational simplicity and efficiency of two-equation models but attempt to indirectly incorporate some of the anisotropy dynamics that would otherwise be accounted for in full Reynolds stress transport models.

By contrast, here we will replace the equilibrium anisotropy expression in Eq. (6) with an alternative closure that is comparably simple, and thus can be readily implemented in existing computational frameworks that are built around Eq. (6), but provides a substantially higher-fidelity representation for the Reynolds stress anisotropy a_{ij} in nonequilibrium turbulence than do current nonlinear models or other direct Reynolds stress models that have been proposed to date.

B. Nonequilibrium anisotropy effects

The Boussinesq closure in Eq. (6) is fundamentally an equilibrium expression that assumes the anisotropy tensor a_{ij} to depend only on the local instantaneous value of the mean strain rate tensor $\bar{S}_{ij}$. Such a representation thus fares poorly when nonequilibrium effects are significant, namely, when temporal or spatial variations in flow properties create large Lagrangian time variations in the strain rate. As will be discussed in Sec. III, the underlying dynamics of the anisotropy tensor then cannot remain in equilibrium with the rapidly changing mean strain rate tensor, and the direct proportionality in Eq. (6) becomes inaccurate.

For instance, simulations of periodically sheared homogeneous turbulence[8] show a clear phase lag between the applied shear and the turbulence anisotropy, whereas the equilibrium Boussinesq closure in Eq. (6) requires the two to always remain in phase. In other nonequilibrium flows,[9–11] a similar lag between a rapidly changing applied strain rate and the response in the turbulence anisotropy is also observed, which the equilibrium nature of the closure in Eq. (6) is fundamentally unable to account for.

Even nonlinear closure representations for the anisotropy tensor a_{ij}, of the type noted in Sec. I A, are unable to account for such nonequilibrium effects. Most such nonlinear models still only relate the Reynolds stresses to the local instantaneous mean strain and rotation rate tensors, and thus are fundamentally still equilibrium closure representations. Such closures are therefore as insensitive to certain nonequilibrium effects as is the classical Boussinesq equilibrium closure in Eq. (6). Owing to the failure of linear and nonlinear equilibrium closures in nonequilibrium turbulence, Reynolds stress transport models or LESs have been generally regarded as the only viable solution approaches for simulating such flows.

Here, however, we develop a new anisotropy closure that seeks to include the principal nonequilibrium dynamics of a_{ij} but that can be readily implemented within existing two-equation computational frameworks based on the classical equilibrium closure in Eq. (6). This is done by formulating a replacement for the local instantaneous mean strain rate $\bar{S}_{ij}$ that appears in the equilibrium closure with a *nonequilibrium effective* strain rate $\tilde{S}_{ij}$ that depends on the straining history of the flow. In particular, by considering the relation between the Reynolds stresses and the vorticity and using a linearized analysis of the nonequilibrium vorticity dynamics in the frame of a translating and rotating material element subjected to time-varying imposed strain rate $S_{ij}(t)$, we express the time response in the vorticity alignment relative to the imposed strain rate eigenvectors as a convolution integral over the strain history to which such individual material elements have been subjected. The anisotropy tensor a_{ij} then results from the ensemble average over the elements arriving at the location $\mathbf{x}$ at the time t in all realizations of the same turbulent flow. This produces a linear closure relation analogous to Eq. (6) but with the resulting ensemble-averaged effective strain rate tensor $\tilde{S}_{ij}$ appearing in place of the mean strain rate $\bar{S}_{ij}$. We show how this result can be obtained from the transport equation for the Reynolds stress anisotropy a_{ij} and how the resulting nonequilibrium anisotropy closure is related to various prior anisotropy models. When this simple nonequilibrium closure is applied to a range of nonequilibrium test cases, it shows substantial improvements over the

classical equilibrium closure and over existing direct approaches for including nonequilibrium effects in Reynolds stress closures.

II. TWO-EQUATION CLOSURE FORMULATIONS

The nonequilibrium anisotropy closure developed herein is formulated as a replacement for the equilibrium closure in Eq. (6). Thus, for example, it can be implemented in essentially any two-equation turbulence model, such as the k-ϵ model,[12] k-ω model,[13] and blended k-ϵ/k-ω model.[14] Due to the widespread familiarity with the standard k-ϵ (SKE) model and the fact that other nonequilibrium closures have been cast in a similar framework, the present nonequilibrium closure will be demonstrated and evaluated within the framework of the k-ϵ model. This is done solely to compare the performance of this new nonequilibrium closure with the conventional equilibrium closure in Eq. (6) and does not represent any inherent limitation in the applicability of the model.

A. The k and ϵ equations

In two-equation k-ϵ formulations, the eddy viscosity in Eq. (6) is represented in terms of the turbulence kinetic energy k and the kinetic energy dissipation rate ϵ, and thus on dimensional grounds must be

$$\nu_T = C_\mu \frac{k^2}{\epsilon}, \tag{7}$$

where C_μ is a constant. The closure is completed by the inclusion of two modeled transport equations for k and ϵ, usually written as

$$\frac{Dk}{Dt} = P - \epsilon + \frac{\partial}{\partial x_j}\left[\left(\nu + \frac{\nu_T}{\sigma_k}\right)\frac{\partial k}{\partial x_j}\right], \tag{8}$$

$$\frac{D\epsilon}{Dt} = C_{\epsilon 1} P \frac{\epsilon}{k} - C_{\epsilon 2}\frac{\epsilon^2}{k} + \frac{\partial}{\partial x_j}\left[\left(\nu + \frac{\nu_T}{\sigma_\epsilon}\right)\frac{\partial \epsilon}{\partial x_j}\right], \tag{9}$$

in which the kinetic energy production rate P for incompressible flows ($\bar{S}_{ii} \equiv 0$) is

$$P \equiv -\overline{u_i' u_j'}\bar{S}_{ij} = -k a_{ij}\bar{S}_{ij}. \tag{10}$$

Standard values[12] of the model constants are

$$C_\mu = 0.09, \quad C_{\epsilon 1} = 1.44, \quad C_{\epsilon 2} = 1.92, \quad \sigma_k = 1.0, \quad \sigma_\epsilon = 1.3. \tag{11}$$

B. Equilibrium standard k-ϵ and realizable k-ϵ implementations

When the equilibrium closure in Eq. (6) is used for the anisotropy a_{ij} with the eddy viscosity in Eq. (7), the resulting equilibrium k-ϵ model represents the Reynolds stress anisotropy as

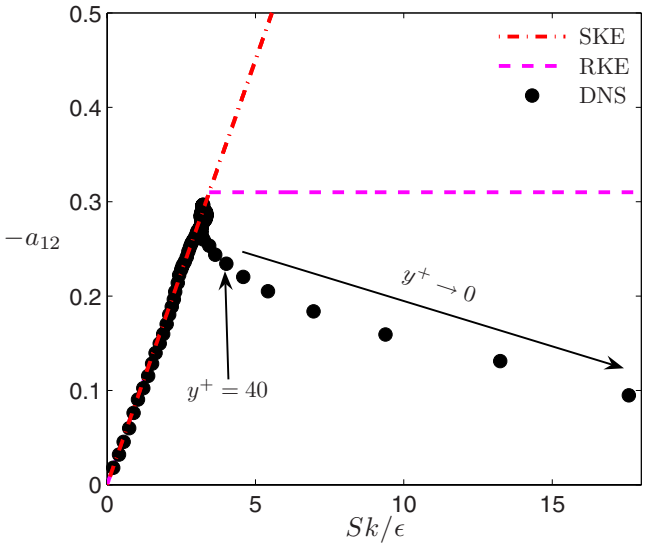

FIG. 1. (Color online) Variation in anisotropy component $-a_{12}$ with Sk/ϵ in turbulent channel flow, showing good agreement of linear form from equilibrium k-ϵ models (SKE and RKE) in Eq. (12) with DNS results of Kim *et al.* (Ref. 15) for Sk/ϵ values outside the near-wall region.

$$a_{ij} = -2C_\mu \frac{k}{\epsilon}\bar{S}_{ij} = -2C_\mu\left(\frac{Sk}{\epsilon}\right)\frac{\bar{S}_{ij}}{S}, \tag{12}$$

where $S \equiv (2\bar{S}_{ij}\bar{S}_{ji})^{1/2}$ characterizes the mean strain rate magnitude. The equilibrium form of this SKE model is relatively successful in turbulent flows where Lagrangian derivatives of flow properties such as k and ϵ are sufficiently small, such as in channel flow or other thin shear flows. Indeed, Fig. 1 shows close agreement for small values of Sk/ϵ between DNS results[15] and the SKE model in a fully developed turbulent channel flow. In particular, the linear variation in Eq. (12) of a_{ij} with the relative strain (Sk/ϵ) is seen to be in good agreement with the DNS data across most of the channel. In the near-wall region where Sk/ϵ becomes large, the agreement becomes poor, and thus somewhat closer agreement is often forced by limiting C_μ in Eq. (11) via the Bradshaw hypothesis as

$$C_\mu = \begin{cases} 0.09 & \text{for } Sk/\epsilon \le 3.4 \\ 0.31(Sk/\epsilon)^{-1} & \text{for } Sk/\epsilon > 3.4 \end{cases} \tag{13}$$

to yield a partially realizable k-ϵ (RKE) model. The SKE and RKE models outlined in Eqs. (7)–(13) for implementing the equilibrium anisotropy closure in Eq. (6) will be used for comparisons with the nonequilibrium closure developed herein.

C. The k and ϵ equations in homogeneous flows

The assessments presented in Sec. IV of the equilibrium closure in the SKE and RKE models and the present nonequilibrium closure are for tests in various homogeneous turbulent flows, for which the k and ϵ equations in Eqs. (8) and (9) become substantially simpler. Since $\partial/\partial x_j(\overline{\ }) \equiv 0$ in homogeneous turbulence, the time evolution of the Reynolds stress tensor becomes decoupled from the first-order single-point

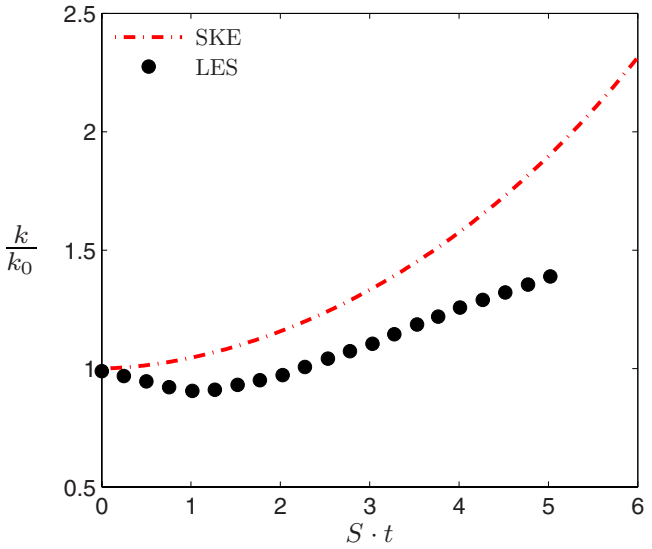

FIG. 2. (Color online) Evolution of turbulence kinetic energy $k(t)/k_0$ for initially isotropic impulsively sheared homogeneous turbulence with $Sk_0/\epsilon_0=3.4$, showing failure of equilibrium k-ϵ (SKE) model in predicting initial nonequilibrium response in $k(t)$ from LES results of Bardina *et al.* (Ref. 9).

moment equations in Eqs. (1)–(3). Moreover, for a given applied strain rate tensor $\bar{S}_{ij}(t)$, the equations for $k(t)$ and $\epsilon(t)$ in Eqs. (8) and (9) reduce to

$$\frac{dk}{dt} = -ka_{ij}\bar{S}_{ij} - \epsilon, \tag{14}$$

$$\frac{d\epsilon}{dt} = -C_{\epsilon 1}\epsilon a_{ij}\bar{S}_{ij} - C_{\epsilon 2}\frac{\epsilon^2}{k}. \tag{15}$$

For a given $\bar{S}_{ij}(t)$ the resulting $k(t)$ and $\epsilon(t)$ are found from Eqs. (14) and (15), with the anisotropy $a_{ij}(t)$ given by Eq. (12) for the equilibrium SKE and RKE models as outlined above.

D. Performance of equilibrium closure in nonequilibrium turbulence

Figure 2 shows the performance of the equilibrium anisotropy closure in the SKE model for the case of initially isotropic homogeneous turbulence with $k=k_0$ and $\epsilon=\epsilon_0$ at $t=0$ that is suddenly subjected for $t>0$ to homogeneous mean shear with relative magnitude $Sk_0/\epsilon_0=3.4$. The anisotropy created by the impulsive shear $\bar{S}_{ij}(t)$ leads to changes in $k(t)$, $\epsilon(t)$, and $a_{ij}(t)$. The resulting $k(t)$ from the equilibrium closure is compared with LES results[9] for this case. At relative times $St \gg 1$, both LES and the equilibrium model show an increase in k with time. However, until $St \approx 2$ there are significant differences between the LES and equilibrium SKE results. In particular, LES shows that the initial response of the turbulence to the impulsively applied shear is a decrease in $k(t)$, while the equilibrium closure in Eq. (12) in the SKE model causes the turbulence kinetic energy to instead increase with time. The difference is due to nonequilibrium effects in the anisotropy response to the applied shear, which are not correctly represented by the Boussinesq equilibrium hypothesis.

Such errors due to nonequilibrium effects will arise whenever Lagrangian time variations in the strain rate $\bar{S}_{ij}(t)$, as well as corresponding variations in k and ϵ, are sufficiently large that the finite time response of the turbulence prevents the anisotropy from reaching equilibrium with the strain rate. As will be seen in Sec. III, such nonequilibrium in the turbulence response can also occur where rotation effects along the mean-flow streamlines are sufficiently large, and even when cross-stream spatial inhomogeneities in the strain and rotation rates are sufficiently large. Since these features commonly arise in practical engineering turbulent flow problems, at least some of the shortcomings of traditional equilibrium turbulence models may be addressed by properly incorporating nonequilibrium effects into the closure scheme.

III. PROPOSED NONEQUILIBRIUM ANISOTROPY CLOSURE

The new nonequilibrium anisotropy closure developed herein seeks to include the finite time response of the turbulence anisotropy noted above but to do so within a comparatively simple direct model for the anisotropy tensor a_{ij}. In the following, a heuristic examination of the physics underlying vorticity dynamics in the presence of varying strain is used to motivate a history-dependent effective strain rate tensor, which is then rigorously derived from the transport equation for the Reynolds stress anisotropy.

A. Physical basis of turbulence anisotropy

The approach taken here is rooted in the dynamics of the vorticity field $\omega_i(\mathbf{x},t)$ under the effect of a strain rate field $S_{ij}(\mathbf{x},t)$. While this is formally equivalent to the dynamics in the transport equation for the Reynolds stress anisotropy tensor a_{ij}, the number of terms that must be approximated in the vorticity transport equation is significantly smaller, and there is a substantial available background on vorticity dynamics that can be used to guide in modeling the effect of these terms on a_{ij}.

The Biot–Savart integral relating the velocity fluctuations to the vorticity fluctuations, namely, the inverse of the vector curl operator, is given by

$$u_i'(\mathbf{x},t) = \frac{1}{4\pi}\int_{\check{\mathbf{x}}} \epsilon_{ijk}\omega_j'(\check{\mathbf{x}},t)\frac{(x_k-\check{x}_k)}{|\mathbf{x}-\check{\mathbf{x}}|^3}d^3\check{\mathbf{x}}, \tag{16}$$

where ϵ_{ijk} is the cyclic permutation tensor. From Eq. (16), the single-point velocity fluctuation correlation can be expressed exactly in terms of the two-point vorticity fluctuation correlation via a double Biot–Savart integral as

$$\overline{u_i'u_j'}(\mathbf{x},t) = \frac{1}{4\pi}\int_{\check{\mathbf{x}}}\frac{1}{4\pi}\int_{\hat{\mathbf{x}}} \epsilon_{ikl}\epsilon_{jmn}\overline{\omega_k'(\check{\mathbf{x}},t)\omega_m'(\hat{\mathbf{x}},t)} \times \frac{(x_l-\check{x}_l)}{|\mathbf{x}-\check{\mathbf{x}}|^3}\frac{(x_n-\hat{x}_n)}{|\mathbf{x}-\hat{\mathbf{x}}|^3}d^3\check{\mathbf{x}}d^3\hat{\mathbf{x}}. \tag{17}$$

It is apparent from Eq. (17) that the two-point vorticity fluc-

tuation correlation determines the Reynolds stresses, and thus the anisotropy a_{ij}. However, the vorticity fluctuation correlation, being a small-scale quantity, is in turn fundamentally determined by the *relative alignment* of the vorticity field $\omega_i(\mathbf{x},t)$ at relatively closely spaced points. Thus, physical insights into the anisotropy evolution can be gained from consideration of the vorticity alignment, which is governed by the substantially simpler transport equation

$$\frac{D\omega_i}{Dt} = \omega_j S_{ij} + \nu\nabla^2\omega_i. \tag{18}$$

The nonlinear dynamics in Eq. (18) enter through the inertial stretching term on the right-hand side, which introduces a dependence on the instantaneous strain rate tensor $S_{ij}(\mathbf{x},t)$.

To understand the effect of the strain rate S_{ij} on the alignment of the vorticity ω_i, it is common to consider a small material element containing a segment of a typical vortical structure into which the vorticity is naturally concentrated at large Reynolds numbers by the competing effects of the stretching and diffusion terms in Eq. (18). The strain rate field within such an element can be separated[16–19] into the *local* strain rate field S_{ij}^L induced within the element by the local vorticity inside the element and the *background* strain rate field S_{ij}^B induced within the element by all the remaining (nonlocal) vorticity outside the element as

$$S_{ij}(\mathbf{x},t) = S_{ij}^L(\mathbf{x},t) + S_{ij}^B(\mathbf{x},t). \tag{19}$$

The background strain S_{ij}^B reflects the largely linear influence of all the surrounding vorticity on the element; this provides only a relatively weak and indirect nonlinear coupling due to the effect of the local vorticity on the nonlocal vorticity. The direct nonlinearity in the vorticity dynamics is due to the local strain S_{ij}^L, through which the structure acts on itself. As noted in Ref. 19 the instantaneous vorticity vector naturally rotates toward alignment with the most extensional eigenvector of the background strain field S_{ij}^B, while the local strain rate field S_{ij}^L induced by any vortical structure has almost no component along the vorticity vector direction. It is primarily through local curvature in the vortical structure that the effect of the local strain on the local vorticity becomes significant. Indeed, for axisymmetric (linelike) and planar (sheetlike) vortical structures[20] the local strain S_{ij}^L may be large but has no component that interacts with the local vorticity.

This suggests that in much of the flow the local dynamics of the vorticity field can be represented as a linear inviscid process governed by the imposed nonlocal background strain $S_{ij}^B(\mathbf{x},t)$, namely,

$$\frac{D\omega_i}{Dt} \approx \omega_j S_{ij}^B. \tag{20}$$

Key features of the nonequilibrium vorticity alignment dynamics in turbulence can be seen in Eq. (20). For slowly varying $S_{ij}^B(\mathbf{x},t)$, the vorticity vector will rotate toward alignment with the most extensional principal axis of the background strain rate tensor—this is typically the intermediate principal axis of the *combined* strain rate tensor in Eq. (19).[19] So long as $S_{ij}^B(\mathbf{x},t)$ varies sufficiently slowly, the vorticity will remain in this equilibrium alignment with the background strain rate tensor. However, when the background strain rate $S_{ij}^B(\mathbf{x},t)$ changes rapidly, then in a frame aligned with the new eigenvectors of S_{ij}^B the short-time dynamics in Eq. (20) leads to an exponential reorientation of the vorticity, on the reorientation time scale $1/S^B$ where $S^B \equiv (2S_{ij}^B S_{ij}^B)^{1/2}$, toward the new most extensional principal axis of S_{ij}^B.

From this quasilinearized model of the local vorticity orientation dynamics in a small material element, we now consider a Lagrangian element that is large enough to contain many such concentrated vortical structures and thereby allows a spatial average within it to define the anisotropy tensor $a_{ij}(t)$ as well as the kinetic energy $k(t)$ and dissipation rate $\epsilon(t)$. In the absence of any preferred direction imposed by the strain rate tensor S_{ij}^B acting on the element, the self-induced and mutual straining of the vortical structures produces a characteristic local strain rate ϵ/k that leads to randomization of the vorticity vector orientations within the element, and thus $a_{ij}=0$. We then examine the impulse response of the anisotropy in this element by imposing a large background strain, specifically $S^B k/\epsilon \to \infty$, over a short duration. Since $S^B \gg \epsilon/k$ during the impulse, the vortical structures must all align on the time scale $1/S^B$ with the most extensional principal axis of S_{ij}^B. For the resulting completely aligned vorticity field, the anisotropy a_{ij} then attains its maximum value. Once the imposed strain is relaxed, the self-induced and mutual straining of the vortical structures gradually returns the random orientations of the vorticity vectors within the element on the time scale k/ϵ, so that $a_{ij} \to 0$. This impulse response of the vorticity alignment in the turbulence suggests a linearized description of turbulence anisotropy dynamics for an arbitrary imposed strain rate S_{ij}^B.

To formalize this, we return to the original small material element, where the dynamics are essentially linear due to Eq. (20), but rather than examining a single element we now consider the ensemble of elements—one from each realization of the flow for the same nominal initial and boundary conditions—that arrive at location $\mathbf{x}$ at time t, as indicated in Fig. 3. Each element arrives along a different pathline, and thus has been subjected to a different straining history $S_{ij}^B(\tau)$, where the time τ identifies the position along the pathline. The ensemble average over all elements at time t now defines the anisotropy tensor, and from the above considerations it is apparent that the resulting $a_{ij}(\mathbf{x},t)$ will not be proportional to the local instantaneous ensemble average of S_{ij}^B at location $\mathbf{x}$ and time t. Rather, if we seek an *effective* strain rate $\tilde{S}_{ij}$ so that $a_{ij} \sim \tilde{S}_{ij}$, then motivated by the above considerations of the impulse response in the vorticity alignment we can regard the vorticity dynamics and associated turbulence anisotropy as a linear system, having the ensemble average of the straining history, denoted $\langle S_{ij}^B(\tau)\rangle$, as its input, $h(t-\tau)$ as its impulse response, and a_{ij}—or equivalently $\tilde{S}_{ij}$—as its output. From linear system theory, the output will be a convolution of the input $\langle S_{ij}^B(\tau)\rangle$ with the impulse response $h(t-\tau)$, and thus the effective strain rate will be of the form

$$\tilde{S}_{ij}(\mathbf{x},t) = \int_{-\infty}^{t} \langle S_{ij}^{B}(\tau)\rangle_{R(\tau)} h(t-\tau) D\tau. \tag{21}$$

Here $\langle S_{ij}^{B}(\tau)\rangle_{R(\tau)}$ is the ensemble average over all elements at time τ along their individual pathlines, as indicated in Fig. 3. This ensemble average is closely related[19] to the mean strain rate $\bar{S}_{ij}$ appearing in standard anisotropy closures, and from the formal derivation in Sec. III B, $\langle S_{ij}^{B}(\tau)\rangle_{R(\tau)}$ appearing in Eq. (21) will be replaced by $\bar{S}_{ij}(\tau)$.

Note that as the material elements in Fig. 3 translate, they also rotate with the local average rotation rate tensor,

$$-\bar{\Omega}_{ij} \equiv \frac{1}{2}\left(\frac{\partial \bar{u}_i}{\partial x_j} - \frac{\partial \bar{u}_j}{\partial x_i}\right), \tag{22}$$

the elements of which are the components of the average vorticity vector within the element. The vortical structures within the element rotate with this mean rotation tensor $\bar{\Omega}_{ij}$, and thus at earlier times τ in Fig. 3 the orientation of the vortical structures differs from that at time $\tau=t$. The rate of change in the anisotropy is determined by the relative alignment of these structures with the background strain rate tensor S_{ij}^{B}. As a consequence, in Eq. (21) the components of the background strain rate tensor $\langle S_{ij}^{B}(\tau)\rangle_{R(\tau)}$ must be given in the coordinate frame of the element at time τ.

In Sec. III B, the heuristic result in Eq. (21) is derived more formally from the transport equation for a_{ij}. The linearization of the a_{ij} dynamics, while historically done for other reasons, is here motivated by the quasilinearized vorticity dynamics in Eq. (20) and will be seen below to produce a result for the effective strain rate $\tilde{S}_{ij}$ analogous to Eq. (21).

B. The effective strain rate tensor

From the definition of the Reynolds stress anisotropy tensor in Eq. (5), the a_{ij} transport equation can be obtained from

$$\frac{Da_{ij}}{Dt} = \frac{1}{k}\left(\frac{D\overline{u_i' u_j'}}{Dt} - \frac{\overline{u_i' u_j'}}{k}\frac{Dk}{Dt}\right). \tag{23}$$

On the right-hand side, the transport equation for the Reynolds stress tensor $\overline{u_i' u_j'}$ can be written[1,3,5,21] as

$$\frac{D\overline{u_i' u_j'}}{Dt} = P_{ij} + \Phi_{ij} - \epsilon_{ij} + D_{ij}, \tag{24}$$

where P_{ij} is the production tensor, Φ_{ij} is the pressure-strain correlation tensor, ϵ_{ij} is the dissipation rate tensor, and D_{ij} accounts for viscous and turbulent transport. The corresponding transport equation for the turbulence kinetic energy k is obtained from the trace of Eq. (24) and is given by

$$\frac{Dk}{Dt} = P - \epsilon + D, \tag{25}$$

where P is defined in Eq. (10), $D \equiv D_{nn}/2$, and $\Phi_{nn} \equiv 0$ in Eq. (24). Substituting Eqs. (24) and (25) into Eq. (23) and employing the definition of the anisotropy tensor in Eq. (5) gives the anisotropy transport equation

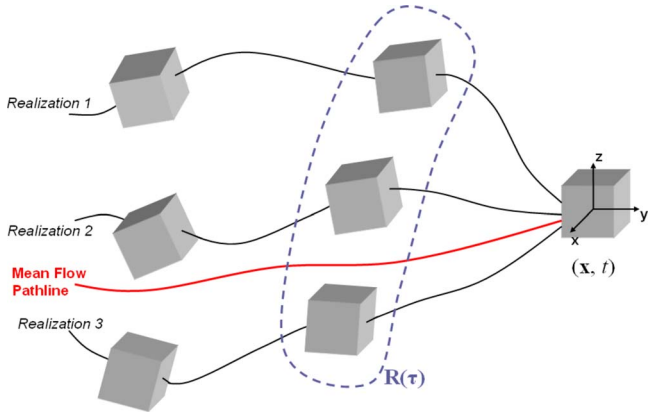

FIG. 3. (Color online) Schematic showing material elements arriving at $(\mathbf{x},t)$ along different pathlines in three representative realizations of the same turbulent flow. Anisotropy $a_{ij}(\mathbf{x},t)$ results from ensemble average over all elements at $(\mathbf{x},t)$, and thus reflects vorticity alignments due to different straining histories along different pathlines. $R(\tau)$ shows representative ensemble of all elements at earlier time τ, revealing effect of strain and rotation histories of mean-flow streamline on $a_{ij}(\mathbf{x},t)$.

$$\frac{Da_{ij}}{Dt} = -\left(\frac{P}{\epsilon} - 1\right)\frac{\epsilon}{k}a_{ij} + \frac{1}{k}\left[P_{ij} - \frac{2}{3}P\delta_{ij}\right] + \frac{1}{k}\Pi_{ij} + \frac{1}{k}\left[D_{ij} - \left(a_{ij} + \frac{2}{3}\delta_{ij}\right)D\right], \tag{26}$$

where the dissipation rate tensor has been decomposed[5] into its isotropic (ϵ) and deviatoric $(\epsilon_{ij})_{\text{dev}}$ parts as

$$\epsilon_{ij} = \tfrac{2}{3}\epsilon\delta_{ij} + (\epsilon_{ij})_{\text{dev}} \tag{27}$$

and where

$$\Pi_{ij} \equiv \Phi_{ij} - (\epsilon_{ij})_{\text{dev}}. \tag{28}$$

The production term in Eq. (26) can be fully expanded in terms of a_{ij}, $\bar{S}_{ij}$, and the antisymmetric part of the mean velocity gradient tensor $\bar{W}_{ij}$, where $\bar{W}_{ij} \equiv -\bar{\Omega}_{ij}$ from Eq. (22), as

$$\left[P_{ij} - \tfrac{2}{3}P\delta_{ij}\right] = -\tfrac{4}{3}k\bar{S}_{ij} - k\left(a_{il}\bar{S}_{lj} + \bar{S}_{il}a_{lj} - \tfrac{2}{3}a_{nl}\bar{S}_{nl}\delta_{ij}\right) + k(a_{il}\bar{W}_{lj} - \bar{W}_{il}a_{lj}). \tag{29}$$

Typically the pressure-strain correlation Π_{ij} in Eq. (26) is modeled as a tensorial expansion in terms of a_{ij}, $\bar{S}_{ij}$, and $\bar{W}_{ij}$. This is given[1,5,22] by the expression

$$\Pi_{ij} = -C_1\epsilon a_{ij} + C_2 k\bar{S}_{ij} + C_3 k\left(a_{il}\bar{S}_{lj} + \bar{S}_{il}a_{lj} - \tfrac{2}{3}a_{nl}\bar{S}_{nl}\delta_{ij}\right) - C_4 k(a_{il}\bar{W}_{lj} - \bar{W}_{il}a_{lj}) + \cdots, \tag{30}$$

where the C_i are constants that may depend on invariants of the $\bar{S}_{ij}$ and $\bar{W}_{ij}$ tensors. Substituting Eqs. (29) and (30) into Eq. (26) and rearranging terms gives the anisotropy transport equation as

$$\frac{Da_{ij}}{Dt} = -\alpha_1 \frac{\epsilon}{k} a_{ij} + \alpha_2 \bar{S}_{ij} + \alpha_3 \left(a_{il}\bar{S}_{lj} + \bar{S}_{il}a_{lj} - \frac{2}{3} a_{nl}\bar{S}_{nl}\delta_{ij} \right) - \alpha_4 (a_{il}\bar{W}_{lj} - \bar{W}_{il}a_{lj}) + \frac{1}{k}\left[D_{ij} - \left(a_{ij} + \frac{2}{3}\delta_{ij} \right) D \right] + \cdots, \tag{31}$$

where

$$\alpha_1 = \frac{P}{\epsilon} - 1 + C_1, \quad \alpha_2 = C_2 - \frac{4}{3}, \quad \alpha_3 = C_3 - 1, \quad \alpha_4 = C_4 - 1. \tag{32}$$

Setting the Lagrangian time derivative on the left-hand side of Eq. (31) to zero, as originally suggested by Pope[23] and Rodi,[24] would discard the explicit nonequilibrium dynamics and lead to the class of algebraic Reynolds stress closures. Within this class, the *linear* equilibrium closure representation in Eq. (6) is obtained by neglecting all terms in Eq. (31) involving higher-order combinations of a_{ij} with $\bar{S}_{ij}$ and $\bar{W}_{ij}$, as well as the D_{ij} transport terms, and solving for a_{ij} in terms of the linear $\bar{S}_{ij}$ term alone. Various *nonlinear* equilibrium models result when the higher-order terms are retained in the closure. For example, Gatski and Speziale,[5] Girimaji,[6] and Wallin and Johansson[7] all derived explicit algebraic models using various equilibrium assumptions, while Yoshizawa,[25] Speziale,[26] Rubinstein and Barton,[27] Taulbee,[28] and Yakhot *et al.*[29] derived nonlinear models based on various expansion methods.

With regard to the present nonequilibrium closure approach, however, we will retain the time derivative on the left-hand side of Eq. (31) and in so doing account for much of the finite time dynamics of the anisotropy tensor. Motivated by the largely linear dynamics that govern the strain-vorticity alignment, and thus the anisotropy, as discussed in Sec. III A, we use the most general form of Eq. (30) that is linear in a_{ij}. Higher-order a_{ij} terms are sometimes retained[22,30] to account for additional aspects of the underlying physics, but it has been noted[31] that these terms are typically small. This gives the weakly nonlinear form of the anisotropy transport equation represented by the terms shown explicitly in Eq. (31). Further consistent with the predominantly linear strain-vorticity alignment dynamics, in this section we retain only the first two terms on the right-hand side of Eq. (31). This gives a quasilinearized dynamical equation for the anisotropy evolution as

$$\frac{Da_{ij}}{Dt} = -\frac{1}{\Lambda_m} a_{ij} + \alpha_2 \bar{S}_{ij}, \tag{33}$$

where we have denoted the resulting turbulence memory time scale Λ_m as

$$\Lambda_m \equiv C_\Lambda \frac{k}{\epsilon} \tag{34}$$

and where

$$C_\Lambda \equiv \frac{1}{\alpha_1}. \tag{35}$$

In the following we will determine a constant value for C_Λ from the nonequilibrium test cases in Sec. IV. The quasilinear form in Eq. (33) is similar to the Maxwell model for linear viscoelastic fluids,[32] where Λ_m is the analogous relaxation time. Note that while there are no retardation terms in Eq. (33) involving material derivatives of $\bar{S}_{ij}$, it may be possible to formulate a more general expansion for the pressure-strain correlation Π_{ij} in Eq. (30) that does account for retardation effects, resulting in a model similar to the Oldroyd or Jeffreys viscoelastic models.[32] In the following, however, we will continue to work with the widely accepted form for Π_{ij} in Eq. (30) and the resulting quasilinear equation in Eq. (33), where retardation effects do not appear.

While the quasilinear equation in Eq. (33) lacks many of the higher-order interactions between a_{ij}, $\bar{S}_{ij}$, and $\bar{W}_{ij}$ on the right-hand side of Eq. (31), it still contains the principal dynamics governing the evolution of the anisotropy in nonequilibrium turbulence, where the mean strain rate varies rapidly with respect to the turbulence response time scale Λ_m. The linearized anisotropy transport equation in Eq. (33) contains both a "slow" $(-a_{ij}/\Lambda_m)$ and a "fast" $(\alpha_2 \bar{S}_{ij})$ contribution to the anisotropy evolution. The fast term accounts for the direct response of turbulence to changes in the mean strain and is often the leading term in rapid distortion analyses of the Reynolds stress anisotropy equation.[21] The slow term represents the vortex scrambling noted in Sec. III A, and thus accounts for the decreasing effect over time of the prior straining history on the local anisotropy. As a result, Eq. (33) addresses the two canonical limits of nonequilibrium turbulence, namely, turbulence subjected to impulsively applied mean strain, where the fast term is dominant, and impulsively removed mean strain, where the slow term is dominant. Equation (33) was originally proposed by Rotta,[33] and was used, for example, by Yakhot *et al.*[29] as the basis for a simple Reynolds stress transport model of the type discussed in Sec. I A, where the six equations for a_{ij} are solved together with the k and ϵ equations.

Here, however, we will integrate Eq. (33) directly to obtain a simpler direct Reynolds stress model that can be readily implemented in the conventional two-equation framework for closing the mean-flow equations in Eqs. (1)–(5). The quasilinear equation in Eq. (33) has an exact solution of the form

$$a_{ij}(t) = \int_{-\infty}^{t} \alpha_2 \bar{S}_{ij}(\tau) e^{-\int_\tau^t [\Lambda_m(t')]^{-1} Dt'} D\tau, \tag{36}$$

where the histories of both $\bar{S}_{ij}$ and the memory time scale Λ_m along a mean-flow pathline are accounted for in the expression for a_{ij}. However, in regions where nonequilibrium effects are large, the Lagrangian time variations in the mean strain rate $\bar{S}_{ij}$ will occur on time scales significantly faster than the turbulence response time scale from the slow term in Eq. (33). In that case, $\Lambda_m(t)$ will be essentially constant with respect to the time scale over which Eq. (33) must be

integrated, and thus the solution for a_{ij} from Eq. (36) becomes a convolution integral of the form

$$a_{ij}(t) = \int_{-\infty}^{t} \alpha_2 \bar{S}_{ij}(\tau) h(t-\tau) D\tau, \tag{37}$$

where $h(\tau)$ is the exponentially decaying impulse response that represents the effective "memory" of the turbulence to its strain history, namely,

$$h(t-\tau) = e^{-(t-\tau)/\Lambda_m(t)}. \tag{38}$$

Note that Eqs. (37) and (38) are consistent with the heuristic result in Eq. (21) from Sec. III A. The present focus on nonequilibrium effects due to the fast term in Eq. (33) distinguishes the present approach from prior nonequilibrium eddy viscosity models,[34–36] which have emphasized nonequilibrium effects related to the time variation in k/ϵ in the slow term and the associated time-varying eddy viscosity $\nu_T(t)$. The closure in Eq. (37) also provides a direct model for the anisotropy, whereas various prior nonequilibrium approaches[29,37,38] require the solution of more extensive sets of coupled differential equations.

By noting[5,35] that C_μ in Eq. (7) is related to the α_i in Eqs. (31) and (32) as

$$C_\mu \equiv -\frac{\alpha_2}{2\alpha_1}, \tag{39}$$

the convolution in Eq. (37) can be equivalently written, with Eqs. (34) and (35), as

$$a_{ij}(t) = -2C_\mu \frac{k}{\epsilon} \frac{1}{\Lambda_m(t)} \int_{-\infty}^{t} \bar{S}_{ij}(\tau) e^{-(t-\tau)/\Lambda_m(t)} D\tau. \tag{40}$$

Since $\Lambda_m(t)$ is a constant with respect to the integration variable τ, the effective strain rate tensor $\tilde{S}_{ij}$ can be defined as

$$\tilde{S}_{ij}(t) = \int_{-\infty}^{t} \bar{S}_{ij}(\tau) \frac{e^{-(t-\tau)/\Lambda_m(t)}}{\Lambda_m(t)} D\tau, \tag{41}$$

in terms of which the nonequilibrium anisotropy closure can be written in a form analogous to the traditional equilibrium closure in Eq. (12) as

$$a_{ij}(t) = -2C_\mu \frac{k}{\epsilon} \tilde{S}_{ij}(t). \tag{42}$$

C. The nonequilibrium anisotropy hypothesis

The relation in Eq. (42) between the anisotropy tensor a_{ij} and the effective strain rate tensor, together with the definition of the eddy viscosity ν_T in Eq. (7), gives

$$a_{ij} = -2\frac{\nu_T}{k} \tilde{S}_{ij}. \tag{43}$$

The result in Eq. (43) is a general nonequilibrium anisotropy closure hypothesis for the Reynolds stresses in turbulent flows that replaces the equilibrium anisotropy closure in Eq. (6). Comparison with Eq. (6) shows that Eq. (43) is still an eddy viscosity formulation and that it differs from the classical Boussinesq equilibrium hypothesis only in that the anisotropy tensor is proportional to the *effective* strain rate tensor $\tilde{S}_{ij}$ in Eq. (41) rather than to the local instantaneous strain rate tensor $\bar{S}_{ij}$. This nonequilibrium closure can thus be readily implemented in essentially any existing computational framework for solving Eqs. (1)–(5) based on an eddy viscosity approach, and modeling of the eddy viscosity ν_T can be done by precisely the same methods as currently used for the Boussinesq equilibrium closure in Eq. (6).

It should be noted that the underlying convolution in Eq. (37) is similar in some respects to a constitutive equation proposed by Crow.[39] In the present approach, however, the vortex scrambling effect that leads to the memory function $h(\tau)$ in the convolution is arrived at in a more natural way from the linear expansion of the pressure-strain correlation in Eq. (30). The Crow model is often cited[22,29,31] for its prediction of α_2 in the fast pressure-strain term in Eq. (33). Here we have used the more recent form in Eq. (30) for the pressure-strain correlation to additionally incorporate effects due to the slow vortex scrambling term in Eq. (33). Several other studies[10,40] have noted the importance of the accumulated strain $\int \bar{S}_{ij}(\tau) d\tau$ in the response of turbulence anisotropy subjected to rapidly varying mean strain. However, this accumulated strain is derived from Eq. (33) by retaining only the fast term $(\alpha_2 \bar{S}_{ij})$, while the exponentially decreasing memory effect in Eq. (41) arises from the slow term $(-a_{ij}/\Lambda_m)$. It has been noted[8] that the slow term is necessary for correctly capturing the physics governing anisotropy evolution in periodically sheared turbulence, and it will be seen in the test cases in Sec. IV that the memory effect in Eq. (41) is an essential aspect of the nonequilibrium response of turbulence anisotropy.

The value of the memory time scale coefficient C_Λ in Eq. (35) can be anticipated from the α_1 values in various prior models. In particular, the stress relaxation model of Yakhot *et al.*,[29] the pressure-strain correlation models of Launder *et al.*[41] and Gibson and Launder,[42] and the explicit algebraic Reynolds stress model of Gatski and Speziale[5] give corresponding values of C_Λ from Eq. (35) shown in Table I (where $P/\epsilon \approx 1.9$ for homogeneous flows was used to calculate α_1). These earlier models thus suggest $C_\Lambda \approx 0.3$; however, the appropriate value of C_Λ for the present nonequilibrium closure will be determined in Sec. IV from various test cases.

TABLE I. Recommended α_1 values and corresponding C_Λ values from various prior closure approaches.

	α_1	C_Λ
Yakhot *et al.* (Ref. 29)	4.4	0.23
Launder *et al.* (Ref. 41)	2.4	0.42
Gibson and Launder (Ref. 42)	2.7	0.37
Gatski and Speziale (Ref. 5)	4.3	0.23

D. Time-local implementation

The effective strain rate $\tilde{S}_{ij}$ was obtained naturally in Eq. (41) in the form of a convolution integral. This can be directly evaluated for given imposed strain rate histories $\bar{S}_{ij}(t)$ in the nonequilibrium tests presented in Sec. IV. However, it does not lend itself readily to implementation in most computational frameworks for solving Eqs. (1)–(5), where only local instantaneous variables are typically available. The integral can, however, be written in an equivalent time-local form that allows $\tilde{S}_{ij}$ to be readily evaluated in such implementations.

The Lagrangian strain rate history term $\bar{S}_{ij}(\tau)$ in the convolution integral in Eq. (41) can be expanded about the current time t as

$$\bar{S}_{ij}(\tau) = \bar{S}_{ij}(t) - \left.\frac{D\bar{S}_{ij}}{Dt}\right|_t (t-\tau) + \frac{1}{2}\left.\frac{D^2\bar{S}_{ij}}{Dt^2}\right|_t (t-\tau)^2 + \cdots. \tag{44}$$

Substituting Eq. (44) in Eq. (41), the effective strain rate can be written as

$$\tilde{S}_{ij}(t) = \int_{-\infty}^{t} \frac{e^{-(t-\tau)/\Lambda_m}}{\Lambda_m}\left[\bar{S}_{ij}(t) - \left.\frac{D\bar{S}_{ij}}{Dt}\right|_t (t-\tau) + \frac{1}{2}\left.\frac{D^2\bar{S}_{ij}}{Dt^2}\right|_t (t-\tau)^2 + \cdots\right] D\tau. \tag{45}$$

Since the derivatives of $\bar{S}_{ij}$ do not depend on τ, Eq. (45) can be written as

$$\tilde{S}_{ij}(t) = \sum_{n=0}^{\infty} \frac{(-1)^n}{n!}\left.\frac{D^n\bar{S}_{ij}}{Dt^n}\right|_t \int_{-\infty}^{t} (t-\tau)^n \frac{e^{-(t-\tau)/\Lambda_m}}{\Lambda_m} D\tau, \tag{46}$$

which then gives

$$\tilde{S}_{ij} = \bar{S}_{ij} + \sum_{n=1}^{\infty} (-\Lambda_m)^n \left.\frac{D^n\bar{S}_{ij}}{Dt^n}\right|_t. \tag{47}$$

The form of the effective strain rate tensor in Eq. (47) is equivalent to the convolution integral in Eq. (41) but allows a time-local evaluation of $\tilde{S}_{ij}$. As an aside, in the general theory of viscoelastic constitutive models, the expansion in Eq. (47) is analogous to the exact series solution for the Maxwell fluid model, in which retardation effects do not appear, and is related to the Rivlin–Erickson constitutive equations for linear viscoelastic fluids.[43] With the nonequilibrium anisotropy hypothesis in Eq. (43), the time-local form in Eq. (47) allows straightforward implementation of the present nonequilibrium model in a computational framework where only local average variables are available.

Note that in obtaining the reduced anisotropy transport equation in Eq. (33), several terms on the right-hand side of Eq. (31) that account for additional effects of the rotation and strain rate tensors on the anisotropy a_{ij} were neglected. However, some of the effects of these terms can be retained by bringing part of their contribution to the left-hand side of Eq. (33) to obtain

$$\frac{\mathring{D}a_{ij}}{Dt} - \frac{\delta_{ij}}{3}\frac{\mathring{D}a_{ll}}{Dt} = -\alpha_1\frac{\epsilon}{k}a_{ij} + \alpha_2\bar{S}_{ij}. \tag{48}$$

where $\mathring{D}/Dt$ is the frame-invariant Oldroyd derivative defined as

$$\frac{\mathring{D}a_{ij}}{Dt} \equiv \frac{Da_{ij}}{Dt} - \frac{\partial\bar{u}_i}{\partial x_l}a_{lj} - \frac{\partial\bar{u}_j}{\partial x_l}a_{li}. \tag{49}$$

Whereas the Lagrangian time derivative on the left-hand side of Eq. (33) accounts for the rate of change in the anisotropy in a frame that translates with the mean flow, the Oldroyd derivative gives the rate of change in a frame that translates, rotates, and deforms with the mean flow, and thus is more fully consistent with the physical picture of turbulence anisotropy noted in Sec. III A.

Within the field of rheology,[32,43,44] constitutive equations related to Eq. (48) that incorporate more complex convective derivatives of the stress tensor often yield integral solutions analogous to Eq. (36). Thus, following similar reasoning to that employed in the derivation of Eq. (47), we can obtain a generalized effective strain that is expressed in time-local form using the Oldroyd derivative as[43]

$$\tilde{S}_{ij} = \bar{S}_{ij} + \sum_{n=1}^{\infty} (-\Lambda_m)^n \left[\frac{\mathring{D}^n\bar{S}_{ij}}{Dt^n} - \frac{\delta_{ij}}{3}\frac{\mathring{D}^n\bar{S}_{ll}}{Dt^n}\right]_t. \tag{50}$$

In this time-local form, the series still gives the nonequilibrium effects as in Eq. (47) but now accounts for some of the effects of rotation and strain from the higher-order terms neglected in the original expansion in Eq. (47).

Note that the first term on the right-hand side in Eq. (47) or Eq. (50) gives the equilibrium response of the flow, and the series accounts for the local nonequilibrium effects on the turbulence anisotropy. The leading $n=1$ term in the series gives the first-order departures from equilibrium, and thus when the local nonequilibrium in the turbulence is sufficiently weak it may be adequate to retain only this term. Where local nonequilibrium effects in the turbulence anisotropy are sufficiently large to exceed this weak limit, additional terms in the series must be retained to adequately account for the effect of the Lagrangian strain rate history. It should be pointed out that the increasingly higher-order derivatives of $\bar{S}_{ij}$ in Eq. (47) or Eq. (50) could potentially affect the numerical stability and convergence properties of a full computational framework for solving the RANS equations with this new nonequilibrium Reynolds stress closure. However, it will be seen in Sec. IV C that truncation of Eqs. (47) and (50) at the $n=1$ term, for which numerical difficulties are not expected to be prohibitive, is sufficient to give substantially improved predictions for the periodically sheared nonequilibrium test case.

IV. TESTS OF THE PROPOSED NONEQUILIBRIUM CLOSURE

Test cases based on homogeneous flows play a key role in turbulence model development since they allow the underlying model physics to be probed directly. The resulting decoupling of the turbulence model from the mean-flow equations allows the anisotropy evolution to be calculated by simple numerical integration of ordinary differential equations, without the need for a full computational framework that can often confuse numerical issues with the performance of the turbulence closure model. In particular, nonequilibrium homogeneous flows are used in this section to conduct a detailed evaluation of turbulence model dynamics in the presence of time-varying imposed mean strain rates $\bar{S}_{ij}(t)$. Such direct assessments of nonequilibrium closure models can be difficult to conduct in the framework of a full computational simulation for various steady and equilibrium mean-flow problems that are often used for turbulence model validation.[40]

Four substantially different nonequilibrium test cases will be addressed here, namely, (i) impulsively sheared homogeneous turbulence, for which LES results are available for comparison from Bardina *et al.*,[9] (ii) periodically sheared homogeneous turbulence, for which computational data are available for comparison from Yu and Girimaji,[8] (iii) strained, relaxed, and destrained homogeneous turbulence, for which experimental data are available for comparison from Chen *et al.*,[11] and (iv) interaction of homogeneous initially isotropic turbulence with a shock wave, for which DNS data are available from Lee *et al.*[45] and Mahesh *et al.*[46] In each case, comparisons of the present nonequilibrium closure hypothesis are made with the Boussinesq equilibrium hypothesis in Eq. (6) via the SKE or RKE models. In all four cases, the imposed strain rate $\bar{S}_{ij}(t)$ allows the effective strain rate $\tilde{S}_{ij}(t)$ in Eq. (41) to be evaluated analytically. For all cases, the prefactor C_Λ in the memory time scale Λ_m in Eq. (34) is the same and given by

$$C_\Lambda \approx 0.26, \tag{51}$$

and thus there are no adjustable constants whatsoever in the nonequilibrium closure. Note that this C_Λ value is in reasonable accord with those in Table I inferred from the α_1 that correspond to various prior closure approaches.

A. Nonequilibrium *k*-ϵ model

In the context of a k-ϵ model, the anisotropy a_{ij} from the present nonequilibrium closure is given by

$$a_{ij} = -2C_\mu \frac{k}{\epsilon}\tilde{S}_{ij} = -2C_\mu \left(\frac{\tilde{S}k}{\epsilon}\right)\frac{\tilde{S}_{ij}}{\tilde{S}}, \tag{52}$$

where $\tilde{S} \equiv (2\tilde{S}_{ij}\tilde{S}_{ji})^{1/2}$. This is similar to Eq. (12) from the equilibrium Boussinesq hypothesis, but here $\bar{S}_{ij}$ and S have been replaced by the corresponding nonequilibrium effective strain rates $\tilde{S}_{ij}$ and $\tilde{S}$. When coupled to the same k and ϵ transport equations in Eqs. (8) and (9) as used for the SKE and RKE models, the resulting system is a nonequilibrium k-ϵ (NKE) model.

Here, this model is applied to predict the turbulence response in the four nonequilibrium homogeneous turbulence test cases. Thus Eqs. (14) and (15) with the standard model constants in Eq. (11) still determine the resulting $k(t)$ and $\epsilon(t)$, but the anisotropy $a_{ij}(t)$ in these equations is now obtained from the nonequilibrium relation in Eq. (52) in place of the equilibrium form in Eq. (12). When implemented in this manner, the resulting NKE model differs from the SKE and RKE models in Sec. II solely due to this new nonequilibrium anisotropy relation for a_{ij}.

B. Impulsively sheared homogeneous turbulence

For the impulsively sheared homogeneous turbulence of Bardina *et al.*,[9] the only nonzero component of the imposed mean strain rate is

$$\bar{S}_{12}(t) = \bar{S}_{21}(t) = \begin{cases} 0 & \text{for } t < 0 \\ S/2 & \text{for } t \geq 0. \end{cases} \tag{53}$$

The equilibrium closure in Eq. (6) with ν_T in Eq. (7) gives the corresponding anisotropy in the SKE model for $t \geq 0$ as

$$a_{12}(t) = a_{21}(t) = -C_\mu \frac{Sk}{\epsilon}. \tag{54}$$

For the present nonequilibrium closure, the effective strain rate $\tilde{S}_{ij}(t)$ from Eqs. (41) and (53) for $t \geq 0$ is

$$\tilde{S}_{12}(t) = \tilde{S}_{21}(t) = (S/2)[1 - e^{-t/\Lambda_m}], \tag{55}$$

and the corresponding anisotropy from Eq. (52) is then

$$a_{12}(t) = a_{21}(t) = -C_\mu \frac{Sk}{\epsilon}[1 - e^{-t/\Lambda_m}]. \tag{56}$$

For the particular case $Sk_0/\epsilon_0 = 3.4$, for which Bardina *et al.*[9] gave LES results, integration of Eqs. (14) and (15) for $k(t)$ and $\epsilon(t)$ from the SKE and NKE models gives the kinetic energy evolution shown in Fig. 4. The history effect in the nonequilibrium closure and the consequent reduction in Eq. (56) of the anisotropy magnitude relative to that in Eq. (54) from the equilibrium closure lower the initial kinetic energy production from the NKE model relative to the corresponding production from the equilibrium closure in the SKE model. This can be seen in Fig. 4 to give an initial reduction in the kinetic energy $k(t)$ from the nonequilibrium closure, in good agreement with the LES results, while the equilibrium closure shows a strictly monotonic increase in $k(t)$.

Due to the initially lower kinetic energy production, $k(t)$ from the nonequilibrium closure in the NKE model is always below that from the equilibrium closure in the SKE model. For $t \gg \Lambda_m$, the nonequilibrium correction to the anisotropy in Eq. (56) becomes negligible, and the kinetic energy production in the NKE model can be seen in Fig. 4 to become similar to that from the equilibrium closure in the SKE model. Thus the nonequilibrium effect that creates the initially lower kinetic energy production remains active only for a time of $O(\Lambda_m)$ after the turbulence is subjected to the

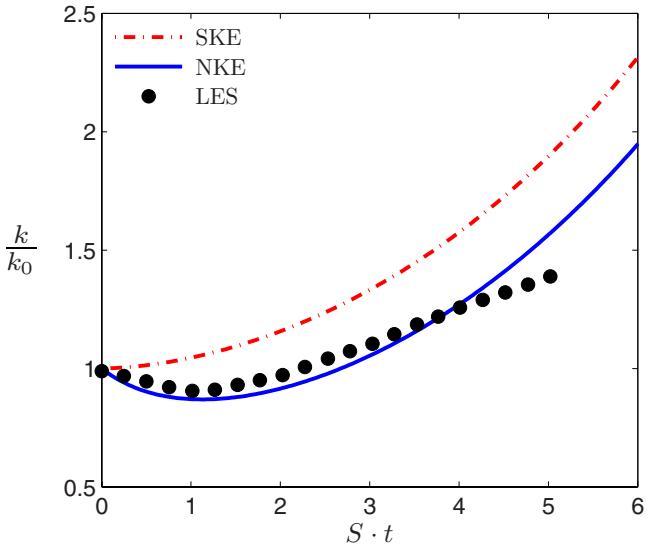

FIG. 4. (Color online) Turbulence kinetic energy $k(t)/k_0$ in initially isotropic impulsively sheared homogeneous turbulence for the same conditions as in Fig. 2, showing that the proposed nonequilibrium closure in the present (NKE) model gives substantially better agreement with the initial nonequilibrium response seen in LES of Bardina *et al.* (Ref. 9) than does classical equilibrium closure in the SKE model.

change in shear. However, this temporary nonequilibrium effect produces a permanent lag in the turbulence response relative to that from the equilibrium closure. This nonequilibrium lag will be seen in the remaining test cases to be a key component of the turbulence response to changes in the mean shear and cannot be accounted for by classical Boussinesq equilibrium closures.

C. Periodically sheared homogeneous turbulence

Tests based on time-periodic shear applied to initially isotropic homogeneous turbulence allow an examination of the nonequilibrium frequency response of the flow. Yu and Girimaji[8] provided simulation results for applied mean strain rates of the form

$$\bar{S}_{12}(t) = \bar{S}_{21}(t) = \begin{cases} 0 & \text{for } t < 0 \\ (S_{\max}/2)\sin(\omega t) & \text{for } t \geq 0, \end{cases} \tag{57}$$

where ω is the shearing frequency and all other components of the mean strain rate tensor are zero. The Boussinesq equilibrium hypothesis in Eq. (6) with ν_T in Eq. (7) then gives the corresponding anisotropy in the SKE model as

$$a_{12}(t) = a_{21}(t) = -C_\mu \frac{S_{\max} k}{\epsilon} \sin(\omega t). \tag{58}$$

From Eqs. (57) and (58), the equilibrium closure thus produces anisotropy that remains in phase with the imposed strain rate and an anisotropy response amplitude that has no direct dependence on the straining frequency ω.

For the nonequilibrium closure, the effective strain rate $\tilde{S}_{ij}(t)$ from Eq. (41) for $t \geq 0$ is

$$\tilde{S}_{12}(t) = \tilde{S}_{21}(t) = \frac{S_{\max}}{2}\left[\frac{1}{1+(\omega\Lambda_m)^2}\right] \times \{\sin(\omega t) - (\omega\Lambda_m)[\cos(\omega t) - e^{-t/\Lambda_m}]\}, \tag{59}$$

and the nonequilibrium anisotropy from Eq. (52) is then

$$a_{12}(t) = a_{21}(t) = -2C_\mu \frac{k}{\epsilon}\tilde{S}_{12}. \tag{60}$$

Thus in contrast to the equilibrium response in Eqs. (57) and (58), the response in Eqs. (59) and (60) from the nonequilibrium closure predicts that, as the relative straining frequency increases, there will be a decrease in the anisotropy amplitude and an increase in the phase difference between the imposed shear and the anisotropy. Additionally, the nonequilibrium closure also predicts a lag in the anisotropy response, analogous to the lag seen in the impulsively sheared test case, but predicts that in this case the lag depends on $\omega\Lambda_m$. This frequency-dependent lag as well as the frequency-dependent phase shift and response amplitude are all missed by classical Boussinesq-like equilibrium closures.

For $S_{\max}k_0/\epsilon_0 = 3.3$ and $\omega/S_{\max} = 0.5$, 1.0, and 10, Yu and Girimaji[8] gave simulation results for the anisotropy response $a_{12}(t)$ shown by the solid curves in Figs. 5(a)–5(c). For the same conditions, integration of Eqs. (14) and (15) for $k(t)$ and $\epsilon(t)$ from the SKE and NKE models yields the corresponding anisotropy evolution also shown in Figs. 5(a)–5(c). Comparisons of these results with the simulations by Yu and Girimaji[8] show that the nonequilibrium closure in the NKE model provides an anisotropy response that agrees far more closely with the simulations than does the Boussinesq equilibrium closure in the SKE model. In particular, as the straining frequency $(\omega/S_{\max})$ increases, the direct decrease in anisotropy amplitude from the nonequilibrium closure as well as the indirect effect from changes in k and ϵ with straining frequency are in overall good agreement with the simulation results. By contrast, the equilibrium closure shows only a far weaker indirect decrease in anisotropy amplitude via the changes in k and ϵ with straining frequency.

In such periodically sheared turbulence, the phase difference between the anisotropy $a_{12}(t)$ and the imposed shear $\bar{S}_{12}(t)$ is of additional interest since any phase lag between the two corresponds to negative turbulence kinetic energy production over part of each period. It is qualitatively apparent in Fig. 5 that the phase response from the nonequilibrium closure is in good agreement with the simulation results, while that from the Boussinesq equilibrium closure is in very poor agreement, particularly at the higher straining frequencies in Figs. 5(b) and 5(c). For both the nonequilibrium closure and the simulations of Yu and Girimaji,[8] the phase lag between the imposed strain and the anisotropy response approaches a constant value once the initial transient has decayed after several straining cycles.

This asymptotic phase lag can be accurately measured at any straining frequency by continuing the integration of Eqs. (14) and (15), with Eq. (58) for the SKE model and with Eq. (60) for the NKE model, to much longer times than those shown in Figs. 5(a)–5(c). The resulting phase lag ϕ for the

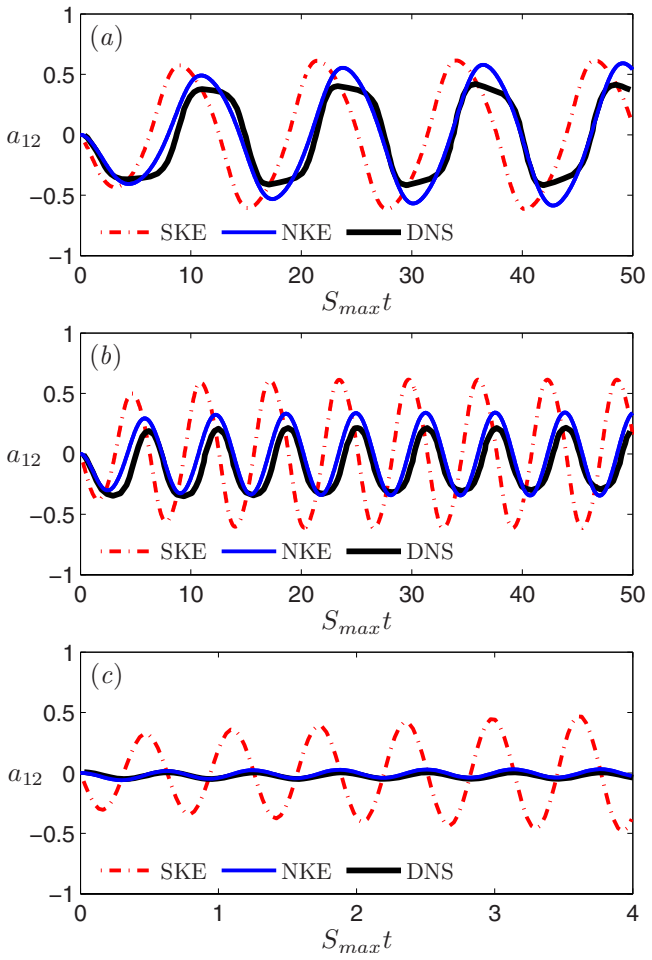

FIG. 5. (Color online) Anisotropy $a_{12}(t)$ in periodically sheared turbulence for relative shearing frequencies $\omega/S_{\max}$=(a) 0.5, (b) 1.0, and (c) 10. For all cases, the proposed nonequilibrium closure in the present (NKE) model gives dramatically improved agreement with corresponding DNS results of Yu and Girimaji (Ref. 8) than does classical equilibrium closure in the SKE model.

equilibrium closure, the nonequilibrium closure, and the simulations of Yu and Girimaji[8] is shown in Fig. 6 over the range of imposed straining frequencies $10^{-2} \leq \omega/S_{\max} \leq 10^{1}$.

For the equilibrium closure in Eqs. (57) and (58), the phase difference from the SKE model is constant at $\phi/\pi=1$ for all frequencies, but this is in very poor agreement with the simulation results in Fig. 6. The nonequilibrium closure in the NKE model, however, shows excellent agreement with the DNS results at all straining frequencies. In the low-frequency limit $\omega/S_{\max} \to 0$, the nonequilibrium closure properly approaches the equilibrium limit in which the imposed straining and the anisotropy response are in phase, and thus $\phi/\pi \to 1$. In the high-frequency limit $\omega/S_{\max} \geq 1$, the nonequilibrium closure properly approaches the saturated nonequilibrium limit, in which the phase difference becomes constant at $\phi/\pi=1/2$. Even more remarkable than the proper approach to these limits is the agreement of the present nonequilibrium closure in the NKE model with the DNS results of Yu and Girimaji[8] for intermediate straining frequencies, where the turbulence is neither in the fully equilibrium or nonequilibrium limits. Only for $\omega/S_{\max} \approx 0.7$, where the turbulence nears the saturated nonequilibrium limit, do the results from the physically based nonequilibrium closure developed herein depart slightly from the simulations.

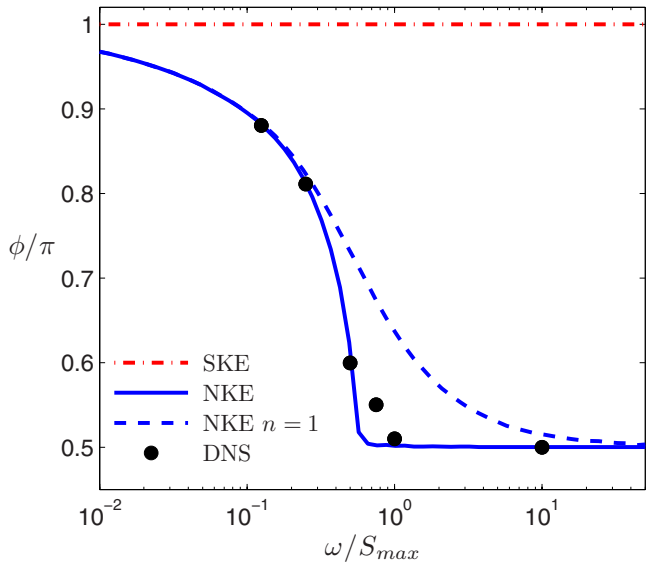

FIG. 6. (Color online) Observed phase difference between anisotropy $a_{12}(t)$ and imposed shear $\bar{S}_{12}(t)$ in periodically sheared turbulence as in Fig. 5, comparing results obtained from the proposed nonequilibrium closure in the NKE model and classical equilibrium closure in the SKE model with the corresponding DNS results from Yu and Girimaji (Ref. 8). The proposed nonequilibrium closure shows good agreement for all frequencies from equilibrium limit to saturated nonequilibrium limit.

In Sec. III D it was noted that numerical difficulties could become significant when retaining higher-order terms in the series expansions of the effective strain rate in Eqs. (47) and (50). It is thus of interest to assess how well the lower-order terms can represent the full nonequilibrium effects. Accordingly, Fig. 6 shows the phase difference obtained when keeping only the lowest-order ($n=1$) term in Eq. (47) or Eq. (50). It is apparent in Fig. 6 that in both the near-equilibrium and saturated nonequilibrium limits, the $n=1$ term suffices to produce the correct phase difference in the resulting turbulence anisotropy. Only at intermediate frequencies does this leading-order term show significant departures from the full nonequilibrium response. This suggests that even with the truncated ($n=1$) form of Eq. (47) or Eq. (50), for which numerical issues are not expected to be prohibitive, the present nonequilibrium closure gives significantly improved predictions of turbulence anisotropy over the classical equilibrium closure.

D. Straining, relaxation, and destraining

An even more complex test of the nonequilibrium turbulence response to an imposed strain rate $\bar{S}_{ij}(t)$ is provided by recent experimental results of Chen *et al.*[11] for the straining, relaxation, and destraining of initially isotropic homogeneous turbulence. In their experiment, $\bar{S}_{22}(t)=-\bar{S}_{11}(t)$ and all other components of the imposed strain rate are zero. Their measured values for the imposed normal strain rate $\bar{S}_{11}(t)$ are given by the symbols in Fig. 7. This straining history can be analytically approximated by the piecewise linear form shown in the same figure, which serves as the input for the

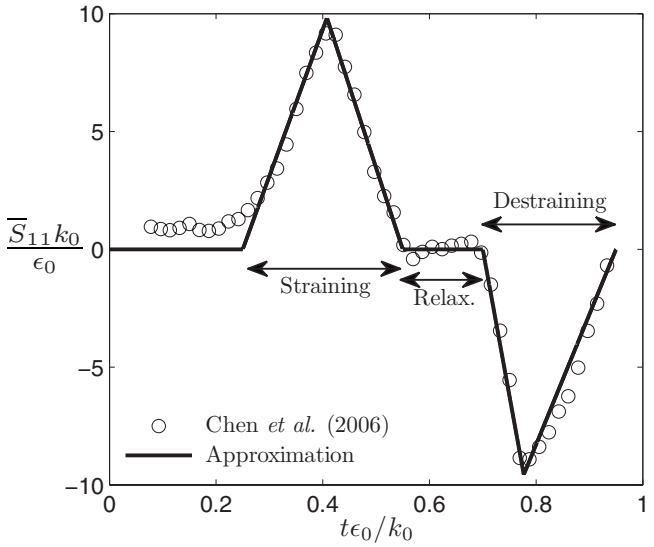

FIG. 7. Imposed mean strain rate $\bar{S}_{11}(t)$ in strained, relaxed, and destrained turbulence experiment of Chen *et al.* (Ref. 11), with piecewise linear approximation used to permit analytical evaluation of equivalent strain rate $\tilde{S}_{11}(t)$ via Eq. (41).

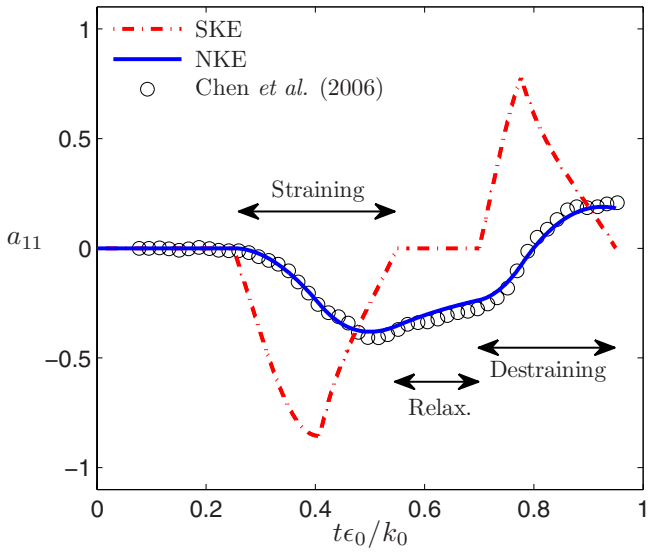

FIG. 8. (Color online) Anisotropy $a_{11}(t)$ in strained, relaxed, and destrained turbulence in Fig. 7, showing comparisons of measured values from Chen *et al.* (Ref. 11) with results from the proposed nonequilibrium closure in the NKE model and from the classical equilibrium closure in the SKE model.

equilibrium and nonequilibrium closures to generate their respective turbulence anisotropy responses $a_{ij}(t)$. The only nonzero components are $a_{11}(t)$ and $a_{22}(t)$, and for the traditional Boussinesq equilibrium closure in the SKE model the resulting anisotropy components are

$$a_{11}(t) = -a_{22}(t) = -2C_\mu \frac{k}{\epsilon}\bar{S}_{11}(t). \tag{61}$$

For the proposed nonequilibrium closure in the NKE model, the effective strain rate $\tilde{S}_{11}(t)$ is obtained via Eq. (41) by integrating the piecewise linear analytical form of $\bar{S}_{11}(t)$ in Fig. 7, and the resulting anisotropy components are then

$$a_{11}(t) = -a_{22}(t) = -2C_\mu \frac{k}{\epsilon}\tilde{S}_{11}(t). \tag{62}$$

For both closures, the respective $a_{ij}(t)$ allows the corresponding $k(t)$ and $\epsilon(t)$ to be obtained by integrating Eqs. (14) and (15).

The results for $a_{11}(t)$ from the SKE and NKE models are shown in Fig. 8, with the measured anisotropy values from Chen *et al.*[11] shown by the symbols for comparison. The measured values were converted from the two-dimensional anisotropy reported by Chen *et al.*[11] to the usual three-dimensional form via isotropy in the unstrained out-of-plane component. The large strain rate values in this test case require the weak realizability constraint in Eq. (13) to limit the C_μ value. Using the average strain rate magnitude in Fig. 7, together with $S=2|S_{11}|$, gives $C_\mu=0.05$. This value is used in both the SKE and NKE models. It is apparent in Fig. 8, however, that even with this realizability constraint the results from the classical Boussinesq equilibrium closure in the SKE model compare very poorly with the measured values from Chen *et al.*[11] This is due to the fact that the equilibrium closure in Eq. (6) assumes the turbulence anisotropy to respond instantaneously to the imposed strain. Thus, for instance, the equilibrium closure predicts zero anisotropy during the relaxation phase.

By contrast, over the entire straining, relaxation, and destraining cycle in Fig. 8 the results from the present nonequilibrium closure in the NKE model can be seen to agree remarkably well with the measured anisotropy values from Chen *et al.*[11] In particular, the nonequilibrium closure correctly predicts a more gradual increase in anisotropy magnitude during the straining phase, as opposed to the rapid increase predicted by the standard equilibrium closure. The nonequilibrium closure then predicts a slow decay of the anisotropy magnitude during the relaxation phase and a gradual increase to positive anisotropy during the destraining phase. The time scales associated with these dynamics show good agreement with the measurements, and the anisotropy values from the NKE model are also in good agreement with the measurements.

Consistent with the results from the impulsively sheared and periodically sheared test cases, these results for straining, relaxation, and destraining of turbulence indicate that the effective strain rate $\tilde{S}_{ij}(t)$ in Eq. (41) and the associated nonequilibrium closure in Eq. (43) capture much of the nonequilibrium dynamics of turbulent flows, and thereby allow most of the advantages of a Reynolds stress transport model to be obtained within the computationally simpler framework of a direct model for the Reynolds stresses.

E. Shock-turbulence interaction

A final test case deals with homogeneous initially isotropic turbulence passing through a shock wave. This is a highly nonequilibrium process that is known[47] to be very poorly predicted by equilibrium models. The interaction is typically represented as steady and one dimensional, and following Sinha *et al.*[47] the dissipation ϵ is taken to have a

negligible effect on the evolution of k and ϵ across the shock. The resulting k transport equation is therefore dominated by kinetic energy production, and thus in a Lagrangian frame becomes

$$\frac{dk}{dt} = -\overline{u'u'}\bar{S}_{11}. \tag{63}$$

The straining imposed as the turbulence passes through the normal shock can be represented by a top-hat function in terms of the pre- and postshock speeds $\bar{u}_1$ and $\bar{u}_2$ and the shock width Δ as

$$\bar{S}_{11} = \lim_{\Delta \to 0} \frac{\bar{u}_2 - \bar{u}_1}{\Delta}, \tag{64}$$

where the straining begins at time t_1 and ends at $t_2 \to t_1$ as $\Delta \to 0$. For all other times $\bar{S}_{11} \equiv 0$. The effective strain rate for $t_1 \leq t \leq t_2$ is thus obtained using Eq. (41) as

$$\tilde{S}_{11}(t) = \lim_{\Delta \to 0} \left(\frac{\bar{u}_2 - \bar{u}_1}{\Delta} \right) [1 - e^{-(t-t_1)/\Lambda_m}]. \tag{65}$$

With the general form of the anisotropy closure in Eq. (43) for a compressible flow, given as

$$a_{ij} = -2\frac{\nu_T}{k}\left(\tilde{S}_{ij} - \frac{1}{3}\tilde{S}_{ll}\delta_{ij} \right), \tag{66}$$

expansion of the exponential contribution to the effective strain rate in Eq. (65) in a Taylor series then allows Eq. (63) to be written as

$$\frac{1}{k}\frac{dk}{dt} = -\frac{2}{3}\left(\frac{\bar{u}_2 - \bar{u}_1}{\Delta} \right) + \frac{4}{3}\frac{C_\mu}{C_\Lambda}\left(\frac{\bar{u}_2 - \bar{u}_1}{\Delta} \right)^2 (t - t_1), \tag{67}$$

where $(t-t_1)/\Lambda_m \to 0$ within the shock removes higher-order terms in the Taylor expansion. Integrating with respect to t and defining $\Delta \equiv U_s(t_2 - t_1)$, where $U_s \equiv \frac{1}{2}(\bar{u}_2 + \bar{u}_1)$ is the characteristic speed through the shock, the turbulence kinetic energy amplification from Eq. (67) is then

$$\frac{k_2}{k_1} = \exp\left[-\frac{4}{3}\left(\frac{1 - \bar{u}_1/\bar{u}_2}{1 + \bar{u}_1/\bar{u}_2} \right) + \frac{8}{3}\frac{C_\mu}{C_\Lambda}\left(\frac{1 - \bar{u}_1/\bar{u}_2}{1 + \bar{u}_1/\bar{u}_2} \right)^2 \right]. \tag{68}$$

As shown in Fig. 9, results from the present nonequilibrium closure in Eq. (68) show closer agreement with the DNS data[45,46] than do either the SKE or RKE model. In particular, for small upstream Mach numbers Fig. 9 shows that the nonequilibrium closure predicts significantly lower kinetic energy amplification across the shock than the SKE model. Moreover, Fig. 9 indicates that the nonequilibrium closure in the NKE model better predicts the kinetic energy amplification k_2/k_1 across the shock at all Mach numbers than does the equilibrium closure in either the SKE or RKE model. For large values of the incoming Mach number M_1, *ad hoc* treatments specific to this problem that provide further reductions in the kinetic energy amplification, as in Ref. 47, can be used to obtain even better agreement with the DNS data.

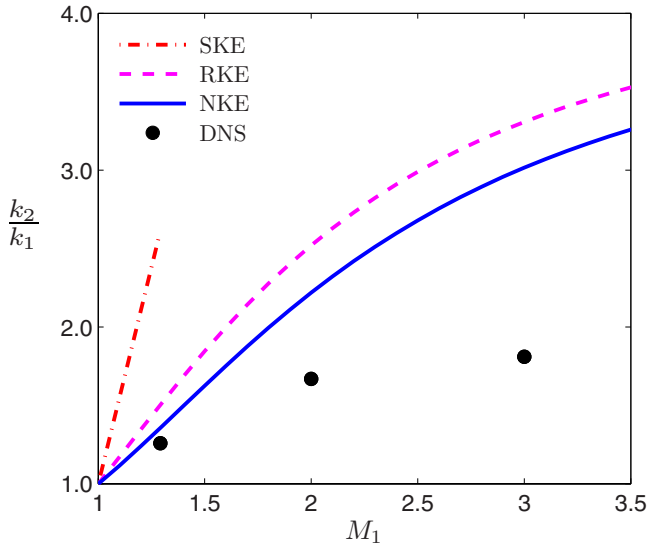

FIG. 9. (Color online) Amplification of turbulence kinetic energy k across a normal shock at various upstream Mach numbers M_1, comparing DNS results (Refs. 45 and 46) with results from the proposed nonequilibrium closure in the NKE model and from the classical equilibrium closure in the SKE (Ref. 47) and RKE models.

V. COMPARISONS WITH PRIOR NONEQUILIBRIUM MODELS

While the nonequilibrium effects in the anisotropy closure developed herein enter naturally through the effective strain rate tensor $\tilde{S}_{ij}$ in Eq. (43), there have been several prior approaches that have sought to introduce nonequilibrium effects within the traditional Boussinesq equilibrium closure via various modifications to the eddy viscosity ν_T in Eq. (6).

For example, Olsen *et al.*[36,48] developed a relatively straightforward nonequilibrium eddy viscosity model that takes into account nonequilibrium effects by solving an additional transport equation for the eddy viscosity as

$$\frac{D\nu_T}{Dt} = a_0\frac{\epsilon}{k}(\nu_{Te} - \nu_T), \tag{69}$$

where $a_0 \approx 3.9$. The parameter ν_{Te} is the equilibrium eddy viscosity, given in Eq. (7) in the context of a k-ϵ implementation, and the transport equation for ν_T in Eq. (69) is then solved with the equations for k and ϵ in Eqs. (8) and (9). However, the Boussinesq equilibrium closure in Eq. (6) is still used to relate the Reynolds stresses to the eddy viscosity ν_T and the mean strain rate tensor $\bar{S}_{ij}$.

The model of Olsen *et al.*[36,48] shows modest improvements over standard equilibrium models for a range of flow problems. However, despite the inclusion of the additional transport equation for ν_T, owing to the equilibrium relation between $a_{ij}(t)$ and $\bar{S}_{ij}(t)$ in Eq. (6) the model cannot predict the lag between the strain rate $\bar{S}_{ij}(t)$ and the resulting anisotropy $a_{ij}(t)$ in periodically sheared turbulence, as shown in Fig. 10. It thus cannot produce the phase differences seen in Figs. 5 and 6 or the lag seen in the experiments and in the NKE model results in Fig. 8. While the additional eddy viscosity transport equation accounts for some nonequilibrium effects, the continued reliance on the instantaneous mean

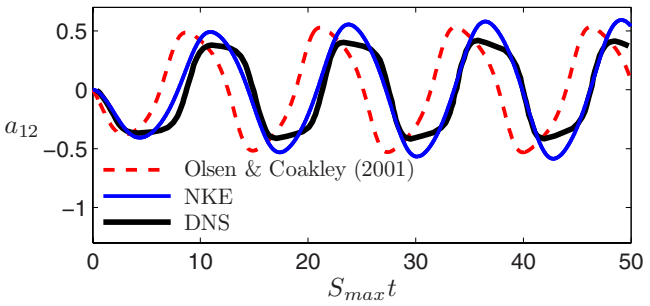

FIG. 10. (Color online) Comparison of anisotropy $a_{12}(t)$ in periodically sheared turbulence at $\omega/S_{\max}=0.5$ from DNS of Yu and Girimaji (Ref. 8) with corresponding results from the nonequilibrium model of Olsen *et al.* (Refs. 36 and 48) and with results from the proposed nonequilibrium closure in the present NKE model.

strain rate tensor in the equilibrium anisotropy closure inherently limits the model in accurately accounting for nonequilibrium effects.

In a somewhat similar approach, Yoshizawa[25] and Yoshizawa and Nisizima[34] proposed a lagged eddy viscosity having the basic form

$$\nu_T = \nu_{Te} - C\frac{k}{\epsilon}\frac{D\nu_{Te}}{Dt}, \tag{70}$$

where ν_{Te} is the equilibrium eddy viscosity in Eq. (7). More recently Yoshizawa *et al.*[35] developed a modified version of the same basic model, in which Eq. (70) is replaced by

$$\nu_T = \begin{cases} \nu_{Te}\left[\Lambda + C_A\frac{1}{k}\frac{D}{Dt}\left(\frac{k^2}{\epsilon}\right)\right]^{-1} & \text{for } \frac{D\nu_{Te}}{Dt} > 0 \\ \nu_{Te}\left[\frac{1}{\Lambda} - \frac{C_A}{\Lambda^2}\frac{1}{k}\frac{D}{Dt}\left(\frac{k^2}{\epsilon}\right)\right] & \text{for } \frac{D\nu_{Te}}{Dt} < 0, \end{cases} \tag{71}$$

where Λ is a dimensionless parameter that depends on Sk/ϵ and Wk/ϵ, with $W \equiv (2\bar{W}_{ij}\bar{W}_{ij})^{1/2}$. However, this approach still uses the equilibrium closure in Eq. (6) to relate the anisotropy $a_{ij}(t)$ to the mean strain rate tensor $\bar{S}_{ij}(t)$. Thus, although this nonequilibrium eddy viscosity model was seen, for example, to improve agreement with DNS results in homogeneous sheared turbulence,[34,35] the phase properties in the resulting anisotropy evolution for periodically sheared turbulence are not substantially different from those in Fig. 10 using the model of Olsen *et al.*[36,48]

Recently Revell *et al.*[49] proposed a novel nonequilibrium k-ϵ-C_{as} eddy viscosity model in which an additional parameter,

$$C_{as} = -\frac{a_{ij}\bar{S}_{ij}}{S}, \tag{72}$$

is used to account for alignment between the Reynolds stress and mean strain rate tensors. In this case, the turbulence kinetic energy production is written as $P=C_{as}kS$, and an additional transport equation is solved to determine C_{as}. This additional equation can be incorporated into standard approaches such as the SKE model, in which case the eddy viscosity becomes

$$\nu_T = k\,\min\left[\frac{C_\mu k}{\epsilon}, \frac{C_{as}}{S}\right], \tag{73}$$

and the usual transport equations in Eqs. (8) and (9) are solved for k and ϵ. However, as with the model of Olsen *et al.*[36,48] and that of Yoshizawa *et al.*,[35] the k-ϵ-C_{as} model fundamentally still employs the Boussinesq equilibrium closure between the anisotropy $a_{ij}(t)$ and the mean strain $\bar{S}_{ij}(t)$. Thus, while the k-ϵ-C_{as} model shows some improvement over the SKE model in predicting the evolution of periodically strained homogeneous turbulence,[49] it still predicts zero anisotropy for zero applied strain, resulting in poor agreement with the DNS data in Fig. 5 and the experimental measurements in Fig. 8 when the applied strain is zero.

All of the prior nonequilibrium models noted above modify the eddy viscosity ν_T to account for nonequilibrium effects but still use the equilibrium closure in Eq. (6) to relate the anisotropy a_{ij} to the mean strain rate $\bar{S}_{ij}$. While such ν_T modifications allow some nonequilibrium effects to be addressed, it is clear that a general nonequilibrium Reynolds stress closure cannot represent the anisotropy a_{ij} as being directly proportional to $\bar{S}_{ij}$ as in Eq. (6) and must take into account the straining history of the turbulence via some method such as the effective strain rate $\tilde{S}_{ij}$ in the present nonequilibrium closure.

VI. RELATION TO NONLINEAR ANISOTROPY MODELS

In order to retain some dependence on the straining history, several prior anisotropy models[25,26,28,50] have included various time derivatives of $\bar{S}_{ij}$ in nonlinear expansions of the anisotropy to obtain the most general closure possible. However, in contrast to the present nonequilibrium closure, which is given in expanded time-local form using Eqs. (43) and (47) as

$$a_{ij} = -2\frac{\nu_T}{k}\bar{S}_{ij} + 2\frac{\nu_T}{k}\Lambda_m\frac{D\bar{S}_{ij}}{Dt} + \cdots, \tag{74}$$

the focus of most prior nonlinear models has not been explicitly on nonequilibrium effects due to Lagrangian variations in the mean strain rate, often to the detriment of the model accuracy in nonequilibrium flows.

For instance, using the most general nonlinear constitutive equation for the Reynolds stress tensor, Speziale[26] devised a nonlinear k-ϵ anisotropy closure of the form

$$a_{ij} = -2C_\mu\frac{k}{\epsilon}\bar{S}_{ij} - 4C_D C_\mu^2\left(\frac{k}{\epsilon}\right)^2\left(\bar{S}_{il}\bar{S}_{lj} - \frac{\delta_{ij}}{3}\bar{S}_{nl}\bar{S}_{nl}\right) - 4C_E C_\mu^2\left(\frac{k}{\epsilon}\right)^2\left(\frac{\mathring{D}\bar{S}_{ij}}{Dt} - \frac{\delta_{ij}}{3}\frac{\mathring{D}\bar{S}_{ll}}{Dt}\right), \tag{75}$$

where $\mathring{D}/Dt$ denotes the Oldroyd derivative defined in Eq. (49) and $C_D=C_E\approx 1.68$. The analogous memory time scale in the Speziale[26] model is $\Lambda_m=2C_EC_\mu(k/\epsilon)$, which comparing with Eq. (34) shows that $C_\Lambda=2C_EC_\mu$. Typically, C_μ is given a value between 0.08 and 0.09, and for this range the Speziale[26] model gives a memory time scale coefficient C_Λ

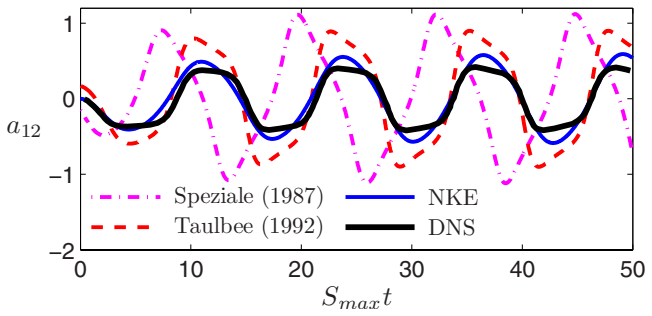

FIG. 11. (Color online) Comparison of anisotropy $a_{12}(t)$ in periodically sheared turbulence at $\omega/S_{\max}=0.5$ from DNS of Yu and Girimaji (Ref. 8) with the corresponding results from Speziale (Ref. 26) and Taulbee (Ref. 28) and the with results from the proposed nonequilibrium closure in the present NKE model.

between 0.27 and 0.30, which is in good agreement with the value $C_\Lambda \approx 0.26$ determined from the wide range of test problems in Sec. IV.

However, in deriving the empirical constants C_E and C_D, Speziale[26] relied on fully developed turbulent channel flow data, for which the material derivative $D\bar{S}_{ij}/Dt$ is zero. This has significant consequences for application of the Speziale[26] model to nonequilibrium flows since the sign accompanying the $\mathring{D}\bar{S}_{ij}/Dt$ term in Eq. (75) is opposite that accompanying the $D\bar{S}_{ij}/Dt$ term in Eq. (74). The discrepancy arises because the Oldroyd derivative was introduced in the Speziale[26] model in an *ad hoc* manner to obtain the most general nonlinear expansion for the Reynolds stress anisotropy, with the coefficient C_E determined from channel flow data where $D\bar{S}_{ij}/Dt=0$. The time derivative of the mean strain rate in Eq. (74), on the other hand, is derived from an expansion of the effective strain rate in Eq. (41), which is itself directly linked to the physics underlying the evolution of the anisotropy, as embodied in Eq. (33).

The effects of the differing signs become especially apparent in periodically sheared turbulence. Using the Speziale[26] model as in Eq. (75), Fig. 11 shows that the phase of the resulting anisotropy is significantly different than in the DNS data and from the NKE model. A similar Reynolds stress model by Huang and Ma[50] also includes a negatively signed Oldroyd derivative term, as in Eq. (75), and is therefore expected to be comparably limited in simulating the anisotropy dynamics in periodically sheared turbulence.

It should be noted that as an intermediate step in the derivation of a nonlinear Reynolds stress model, Taulbee[28] derived an expression for the anisotropy of the form

$$a_{ij} = -2C_\mu \frac{k}{\epsilon}\bar{S}_{ij} - 4\alpha_2\left(\frac{k}{\epsilon}\right)^2(\bar{S}_{il}\bar{W}_{lj} - \bar{W}_{il}\bar{S}_{lj}) - 4\alpha_3\left(\frac{k}{\epsilon}\right)^2\left(\bar{S}_{il}\bar{S}_{lj} - \frac{1}{3}\bar{S}_{nl}\bar{S}_{nl}\delta_{ij}\right) + 4C'_\mu\left(\frac{k}{\epsilon}\right)^2\frac{D\bar{S}_{ij}}{Dt} + \cdots, \tag{76}$$

where the only relevant constant for this discussion is $C'_\mu = \frac{1}{2}(0.35)C_\mu$, where $C_\mu \approx 0.09$ and we have taken $P/\epsilon \approx 1.9$. While the final nonlinear Reynolds stress model devised by Taulbee[28] cannot capture certain nonequilibrium effects due to its dependence on the local and instantaneous values of $\bar{S}_{ij}$ and $\bar{W}_{ij}$, it can be seen that the sign accompanying the $D\bar{S}_{ij}/Dt$ term in the intermediate result in Eq. (76) is positive, in agreement with the present model in Eq. (74). When applied to periodically sheared turbulence the closure in Eq. (76) gives the anisotropy evolution shown in Fig. 11, which is clearly in better agreement with the DNS and NKE model results than is the Speziale[26] model due to the correctly predicted sign accompanying the $D\bar{S}_{ij}/Dt$ term in Eq. (76).

Thus, in the form in Eq. (74) for the present nonequilibrium closure the time derivative of the strain rate results directly from the physics underlying nonequilibrium turbulence anisotropy, resulting in a model that reveals the correct dependence of the anisotropy on time variations in the mean strain rate tensor. Moreover, the coefficient C_Λ associated with this term in Eq. (74) has been determined from a wide range of nonequilibrium flows in Sec. IV, resulting in increased accuracy over prior models that introduce nonequilibrium effects in an *ad hoc* manner.

VII. CONCLUSIONS

We have developed a new anisotropy closure that includes the principal nonequilibrium dynamics of a_{ij} but that can be readily implemented within existing computational frameworks based on the classical Boussinesq equilibrium closure in Eq. (6). This has been done by formulating a replacement for the local instantaneous mean strain rate tensor $\bar{S}_{ij}$ that appears in the equilibrium closure with a nonequilibrium effective strain rate tensor $\tilde{S}_{ij}$ that depends on the strain rate history experienced by material elements in the flow. Considering the relation between the Reynolds stresses and the vorticity suggests a linearized analysis of the nonequilibrium vorticity alignment dynamics in the frame of a translating and rotating material element subjected to time-varying imposed strain rate $S_{ij}(t)$. A formal analysis from the transport equation for a_{ij} gives the anisotropy as a convolution integral over the strain history to which individual material elements have been subjected. In contrast to previous nonequilibrium approaches that have sought to include nonequilibrium effects via direct modifications to the eddy viscosity, here the nonequilibrium effects enter through the resulting history-dependent effective strain rate tensor. The convolution integral for this effective strain rate tensor can be equivalently expressed in a purely time-local form that allows increasingly higher-order nonequilibrium effects to be included by retaining increasingly higher-order terms in the resulting series. The final result for the turbulence anisotropy is in the form of a linear closure relation analogous to Eq. (6), but with the ensemble-averaged effective strain rate tensor $\tilde{S}_{ij}$ appearing in place of the mean strain rate $\bar{S}_{ij}$.

When this nonequilibrium closure in Eq. (43) with Eq. (41) or Eq. (47) or with Eq. (50) was implemented in a NKE model and applied to a range of substantially different test cases, the results showed dramatic improvements over the

classical equilibrium closure in Eq. (6) in the SKE and closely related RKE models. The present nonequilibrium closure also showed substantial improvements over previous direct approaches for including nonequilibrium effects in Reynolds stress closures. In all these tests the same prefactor $C_\Lambda = 0.26$ was used for the memory time scale in Eq. (34), with the consequence that there were no adjustable constants in this nonequilibrium closure. Moreover, this C_Λ value is in reasonable accord with values in Table I inferred from various prior closure approaches. The test cases in Sec. IV showed that, for periodically sheared turbulence in Fig. 5, the present nonequilibrium closure for $a_{ij}(t)$ in terms of the effective strain rate $\tilde{S}_{ij}(t)$ correctly predicts the reduction in anisotropy magnitude and increase in phase lag with increasing straining frequency seen in the DNS results of Yu and Girimaji.[8] As seen in Fig. 6, the phase difference between the strain rate $\bar{S}_{ij}(t)$ and the resulting anisotropy $a_{ij}(t)$ is correctly produced over all straining frequencies from the equilibrium limit to the saturated nonequilibrium limit. Additionally, as seen in Fig. 8, the nonequilibrium closure produces much more accurate time lags and anisotropy magnitudes than the Boussinesq equilibrium closure in the straining, relaxation, and destraining experiment of Chen *et al.*[11] over the entire cycle.

All of these tests were based on homogeneous flows, which allow the turbulence anisotropy to be calculated by numerical integration of ordinary differential equations, without the need for a full computational framework for the mean-flow equations that can often confuse numerical issues with the underlying performance of the turbulence closure. It should be noted, however, that the lack of spatial gradients in such homogeneous flows does not address the effects of some of the terms that were neglected in the quasilinearization in Eqs. (33) and (48) of the Reynolds stress transport equation to provide the effective strain rate tensor in Eqs. (41) and (47) or Eq. (50). It is possible that these terms may contribute significantly to the nonequilibrium effects in some types of flows, where the associated contributions from the remaining production, pressure-strain, and diffusion terms may be important. This issue, however, will require the present closure in Eq. (43) with Eq. (41) or Eq. (47) or with Eq. (50) to be incorporated within a full computational framework for solving the mean-flow equations in Eqs. (1)–(5).

Note that the increasingly higher-order material derivatives in the time-local expansion of the effective strain rate tensor in Eqs. (47) and (50) could potentially affect the numerical stability and convergence properties of a full computational framework for solving the RANS equations with this new nonequilibrium Reynolds stress closure. However as shown in Fig. 6, keeping only the lowest-order $(n=1)$ term, for which numerical issues are not expected to be prohibitive, suffices to produce the correct phase lag in the turbulence anisotropy in both the near-equilibrium and saturated nonequilibrium limits of periodically sheared homogeneous turbulence. At all shearing frequencies, the truncated $(n=1)$ form gives significantly improved predictions of the anisotropy phase lag over the classical equilibrium closure. Inclusion of higher-order terms will further improve the accuracy at intermediate frequencies but could potentially come at the expense of numerical stability. An assessment of the stability and convergence properties of this new nonequilibrium closure must, however, await its implementation in a full computational framework for complex inhomogeneous flows.

ACKNOWLEDGMENTS

This work was supported, in part, by the Air Force Research Laboratory (AFRL) through the Michigan-AFRL Collaborative Center for Aeronautical Sciences (MACCAS) under Award No. FA8650-06-2-3625 and by the National Aeronautics and Space Administration (NASA) Marshall Research Center and Glenn Research Center and the Department of Defense (DoD) under the NASA Constellation University Institutes Project (CUIP) under Grant No. NCC3-989.

[1] C. G. Speziale, "Analytical methods for the development of Reynolds-stress closures in turbulence," Annu. Rev. Fluid Mech. **23**, 107 (1991).
[2] T. B. Gatski, "Constitutive equations for turbulent flows," Theor. Comput. Fluid Dyn. **18**, 345 (2004).
[3] A. V. Johansson, "Engineering turbulence models and their development, with emphasis on explicit algebraic Reynolds stress models," in *Theories of Turbulence: CISM Courses and Lectures No. 442* (Springer, New York, 2002), pp. 253–300.
[4] J. L. Lumley, "Toward a turbulent constitutive relation," J. Fluid Mech. **41**, 413 (1970).
[5] T. B. Gatski and C. G. Speziale, "On explicit algebraic stress models for complex turbulent flows," J. Fluid Mech. **254**, 59 (1993).
[6] S. S. Girimaji, "Fully explicit and self-consistent algebraic Reynolds stress model," Theor. Comput. Fluid Dyn. **8**, 387 (1996).
[7] S. Wallin and A. V. Johansson, "An explicit algebraic Reynolds stress model for incompressible and compressible turbulent flows," J. Fluid Mech. **403**, 89 (2000).
[8] D. Yu and S. S. Girimaji, "Direct numerical simulations of homogeneous turbulence subject to periodic shear," J. Fluid Mech. **566**, 117 (2006).
[9] J. Bardina, J. H. Ferziger, and W. C. Reynolds, "Improved turbulence models based on large-eddy simulation of homogeneous, incompressible turbulent flows," Stanford University Report No. TF-19, 1983; J. Bardina, "Improved turbulence models based on large eddy simulation of homogeneous, incompressible, turbulent flows," Ph.D. thesis, Stanford University, 1983.
[10] I. Hadzic, K. Hanjalic, and D. Laurence, "Modeling the response of turbulence subjected to cyclic irrotational strain," Phys. Fluids **13**, 1739 (2001).
[11] J. Chen, C. Meneveau, and J. Katz, "Scale interactions of turbulence subjected to a straining-relaxation-destraining cycle," J. Fluid Mech. **562**, 123 (2006).
[12] B. E. Launder and D. B. Spalding, "The numerical computation of turbulent flows," Comput. Methods Appl. Mech. Eng. **3**, 269 (1974).
[13] D. C. Wilcox, *Turbulence Modeling for CFD* (DCW Industries, La Canada, CA, 2000).
[14] F. R. Menter, "Two-equation eddy-viscosity turbulence models for engineering applications," AIAA J. **32**, 1598 (1994).
[15] J. Kim, P. Moin, and R. Moser, "Turbulence statistics in fully developed channel flow at low Reynolds number," J. Fluid Mech. **177**, 133 (1987).
[16] Z. S. She, E. Jackson, and S. A. Orszag, "Structure and dynamics of homogeneous turbulence: Models and simulations," Proc. R. Soc. London, Ser. A **434**, 101 (1991).
[17] K. K. Nomura and G. K. Post, "The structure and dynamics of vorticity and rate of strain in incompressible homogeneous turbulence," J. Fluid Mech. **377**, 65 (1998).
[18] J. G. Brasseur and W. Lin, "Kinematics and dynamics of small-scale vorticity and strain-rate structures in the transition from isotropic to shear turbulence," Fluid Dyn. Res. **36**, 357 (2005).

[19]P. E. Hamlington, J. Schumacher, and W. J. A. Dahm, "Local and nonlocal strain rate fields and vorticity alignment in turbulent flows," Phys. Rev. E **77**, 026303 (2008).
[20]K. A. Buch and W. J. A. Dahm, "Experimental study of the fine-scale structure of conserved scalar mixing in turbulent flows. Part 1. $Sc \gg 1$," J. Fluid Mech. **317**, 21 (1996).
[21]S. B. Pope, *Turbulent Flows* (Cambridge University Press, Cambridge, 2000).
[22]C. G. Speziale, S. Sarkar, and T. B. Gatski, "Modeling the pressure strain correlation of turbulence: An invariant dynamical systems approach," J. Fluid Mech. **227**, 245 (1991).
[23]S. B. Pope, "A more general effective-viscosity hypothesis," J. Fluid Mech. **72**, 331 (1975).
[24]W. Rodi, "A new algebraic relation for calculating the Reynolds stresses," Z. Angew. Math. Mech. **56**, T219 (1976).
[25]A. Yoshizawa, "Statistical analyis of the deviation of the Reynolds stress from its eddy-viscosity representation," Phys. Fluids **27**, 1377 (1984).
[26]C. G. Speziale, "On nonlinear k-l and k-ϵ models of turbulence," J. Fluid Mech. **178**, 459 (1987).
[27]R. Rubinstein and J. M. Barton, "Nonlinear Reynolds stress models and the renormalization group," Phys. Fluids A **2**, 1472 (1990).
[28]D. B. Taulbee, "An improved algebraic Reynolds stress model and corresponding nonlinear stress model," Phys. Fluids A **4**, 2555 (1992).
[29]V. Yakhot, S. A. Orszag, S. Thangam, T. B. Gatski, and C. G. Speziale, "Development of turbulence models for shear flows by a double expansion technique," Phys. Fluids A **4**, 1510 (1992).
[30]S. Sarkar and C. G. Speziale, "A simple nonlinear model for the return to isotropy in turbulence," Phys. Fluids A **2**, 84 (1990).
[31]C. G. Speziale and R. M. C. So, *The Handbook of Fluid Dynamics* (Springer, New York, 1998), Chap. 14, pp. 14.1–14.111.
[32]R. B. Bird, R. C. Armstrong, and O. Hassager, *Dynamics of Polymeric Liquids*, 2nd ed. (Wiley, New York, 1987).
[33]J. C. Rotta, "Recent attempts to develop a generally applicable calculation method for turbulent shear flow layers," North Atlantic Treaty Organization Report No. AGARD-CP-93, 1972.
[34]A. Yoshizawa and S. Nisizima, "A nonequilibrium representation of the turbulent viscosity based on a two-scale turbulence theory," Phys. Fluids A **5**, 3302 (1993).
[35]A. Yoshizawa, S. Nisizima, Y. Shimomura, H. Kobayashi, Y. Matsuo, H. Abe, and H. Fujiwara, "A new methodology for Reynolds-averaged modeling based on the amalgamation of heuristic-modeling and turbulence-theory methods," Phys. Fluids **18**, 035109 (2006).
[36]M. E. Olsen and T. J. Coakley, "The lag model, a turbulence model for nonequilibrium flows," AIAA Paper No. 2001-2564, 2001.
[37]T. Jongen and T. B. Gatski, "A unified analysis of planar homogeneous turbulence using single-point closure equations," J. Fluid Mech. **399**, 117 (1999).
[38]C. G. Speziale and X.-H. Xu, "Towards the development of second-order closure models for non-equilibrium turbulent flows," Int. J. Heat Fluid Flow **17**, 238 (1996).
[39]S. C. Crow, "Viscoelastic properties of fine-grained incompressible turbulence," J. Fluid Mech. **33**, 1 (1968).
[40]B. A. Pettersson-Reif, T. B. Gatski, and C. L. Rumsey, "On the behavior of two-equation models in nonequilibrium homogeneous turbulence," Phys. Fluids **18**, 065109 (2006).
[41]B. E. Launder, G. Reece, and W. Rodi, "Progress in the development of a Reynolds stress turbulence closure," J. Fluid Mech. **68**, 537 (1975).
[42]M. M. Gibson and B. E. Launder, "Ground effects on pressure fluctuations in the atmospheric boundary layer," J. Fluid Mech. **86**, 491 (1978).
[43]A. G. Fredrickson, *Principles and Applications of Rheology* (Prentice-Hall, Englewood Cliffs, NJ, 1964).
[44]J. D. Goddard and C. Miller, "An inverse for the Jaumann derivative and some applications to the rheology of viscoelastic fluids," Rheol. Acta **5**, 177 (1966).
[45]S. Lee, S. K. Lele, and P. Moin, "Interaction of isotropic turbulence with shock waves: Effect of shock strength," J. Fluid Mech. **340**, 225 (1997).
[46]K. Mahesh, S. K. Lele, and P. Moin, "The influence of entropy fluctuations on the interaction of turbulence with a shock wave," J. Fluid Mech. **334**, 353 (1997).
[47]K. Sinha, K. Mahesh, and G. V. Candler, "Modeling shock unsteadiness in shock/turbulence interaction," Phys. Fluids **15**, 2290 (2003).
[48]M. E. Olsen, R. P. Lillard, and T. J. Coakley, "The lag model applied to high speed flows," AIAA Paper No. 2005-101, 2005.
[49]A. J. Revell, S. Benhamadouche, T. Craft, and D. Laurence, "A stress-strain lag eddy viscosity model for unsteady mean flow," Int. J. Heat Fluid Flow **27**, 821 (2006).
[50]Y.-N. Huang and H.-Y. Ma, "Reynolds stress model involving the mean spin tensor," Phys. Rev. E **70**, 036302 (2004).